Atmospheric Research 178–179 (2016) 426–444

Contents lists available at ScienceDirect

Atmospheric Research

journal homepage: www.elsevier.com/locate/atmosres

Potential of sequential EnKF for the short-range prediction of a maritime severe weather event

D.S. Carrió *, V. Homar

Universitat de les Illes Balears, Physics Department, Carretera de Valldemossa km 7.5, 07122, Palma de Mallorca, Spain

ARTICLE INFO

Article history:
Received 6 October 2015
Received in revised form 5 April 2016
Accepted 12 April 2016
Available online 29 April 2016

Keywords:
Data assimilation
EnKF
Maritime severe weather
WRF-DART

ABSTRACT

The Western Mediterranean coastlands are persistently affected by severe phenomena related to maritime convective systems. Areas with low density of observations around highly populated regions pose serious forecasting challenges due to the risk of misrepresenting crucial structures. This forecast problem is exemplified by the squall line that affected Mallorca (Spain) on 4th October 2007. Ensemble Kalman Filter (EnKF) assimilation algorithms exploit the statistical information conveyed by ensembles and are specially suited for regions with poor knowledge about climatological error statistics and covariances. We investigate the potential for predictability improvement from the assimilation of standard observations in the squall line event. Ensemble forecasts are assessed in terms of probabilistic products which clearly bring out the differences between assimilation and control experiments. Results show the large improvements rendered by the EnKF system in terms of severe weather threat. The attribution of these improvements is discussed in terms of the environmental ingredients linked to squall line formation. Experiments reveal that forecast improvements are fully attributable to the ability of EnKF to accurately represent the convergent flow over the Alboran Sea responsible for the thunderstorm initiation. Additional sensitivity experiments are performed to confirm the hypothesised primary role of the terrestrial observations in the accurate representation of the low-level convergent flow. These experiments confirm the ability of the sequential assimilation system in conveying crucial observational information from terrestrial to marine areas, and thus bestowing the EnKF a central role in future upgrades of high impact weather prediction systems in the Western Mediterranean region.

1. Introduction

The numerical prediction of high-impact weather over islands and coastal areas remains a global daunting challenge. Observing systems with large in-situ data-void regions, such as maritime areas, critically affect the accuracy of forecasts as important structures are frequently missed in the analyses (Wu et al., 2013). Over the past 40 years, increasingly sophisticated methods have been developed to improve the representation of the atmosphere in numerical weather prediction models from a wealth of observations, both in situ, and most importantly, from remote sensing instruments (Rabier, 2005; Palmer and Hagedorn (2006); Shen et al., 2016). This progress has unquestionably led to significantly reduced errors in the initial fields, and thus to improved numerical predictions, mostly in the medium term (Cacciamani et al., 2000; Courtier et al., 1998; Houtekamer et al., 2005; Bouttier and Kelly, 2001). However, established techniques at synoptic-scale in global forecast systems (Buizza et al., 2005) require reconsideration when transferred to the meso- and convection-allowing scales, due both to the fundamentally different dominant dynamics, and the higher nonlinearity, which produces faster error propagation and growth (Zhang et al., 2003; Hohenegger and Schär, 2007; García-Moya et al., 2011; Vich et al., 2011).

Ensemble Kalman filter (EnKF; Evensen, 1994) has been proposed as the data assimilation technique meant to become a reference for subsynoptic scale prediction systems (Torn, 2010; Stensrud et al., 2013). Data assimilation methods, amongst them EnKF, determine the most likely estimate of the atmospheric state by blending information from an initial guess (background) and a set of observations. Essentially, the EnKF contributes to the data assimilation scene by proposing an ensemble-based method to derive an estimate of the background error covariance matrix used in the Kalman filter (Houtekamer and Mitchell, 2001). In this sense, the EnKF is similar to variational methods, like 3DVAR or 4DVAR (Buehner et al., 2009; Lorenc, 2003), with some important differences found between them. The EnKF is conceptually formulated following a sequential algorithm, as opposed to the iterative variational algorithm used by the 4DVAR. The way the error covariance matrix is evolved or the use of dynamic background-error covariances are also fundamental differences between both approaches. EnKF algorithms have been widely used to initialize limited-area models (Meng and Zhang, 2011, e.g.), and most studies investigate cases initialized and evolved over land. We lay the foundations of this study over the

* Corresponding author.
E-mail address: diego.carrio@uib.es (D.S. Carrió).

http://dx.doi.org/10.1016/j.atmosres.2016.04.011
0169-8095/

hypothesis that cycling ensemble Kalman filters which intensively assimilate observations from coastal regions have a great potential for improving socially relevant phenomena initiated over maritime areas. The ability of cycling data assimilation methods to transport information from relatively well instrumented areas towards maritime regions draws the fundamental motivation for the experiments presented in this paper as not only improves the prediction per-se, but it has the promising potential of making an efficient use of remote sensing observations over the sea.

On 4th October 2007, an intense squall line swept across the Balearic Islands (Fig. 1), producing 3 tornadoes (surveyed by the Spanish Weather Agency, AEMET), severe winds and very high precipitation intensities that produced local floods in Palma. One person was killed by debris, more than 200 people were injured by wind-related incidents and material losses were estimated at several tens of millions of Euros (Ramis et al., 2009). Severe convective storms during autumn are not uncommon in the Western Mediterranean area (Riosalido, 1990; Tudurí and Ramis, 1997) mainly because of two ingredients: convective instability by strong latent heat flux from the relatively warm Mediterranean sea, and the uplift provided by the complex orography of the area when interacting with the impinging low-level flows (Romero et al., 1997; Malguzzi et al., 2006). Historical examples of these severe convective episodes in the Western Mediterranean basin are the tornadoes recorded in Mallorca and Menorca on 26th October 1991 and 8th October 1992 respectively (Gayà and Solio, 1993); the heavy precipitation event with amounts exceeding 800 mm in 24 h on 4th November 1987 in Gandía (Valencia) (Romero et al., 1998); the 6 cm diameter hailfall on 15th August 1954 and on 26th August 1968 in Mallorca (Miró-Granada, 1969), amongst other similar cases (García-Dana et al., 1982; Benet, 1986; Fernández et al., 1995; Ramis and Romero, 1995; Ramis et al., 1994; Homar et al., 2003). The precise short-range prediction of the time, location, and intensity of severe phenomena is still beyond current operational prediction systems. The Spanish Weather Service (AEMET) continuously develops numerical tools, based on data assimilation methods and km scale prediction, for the short-range forecasting of high impact weather events in Spain (Navascués et al., 2013). Ducrocq et al. (2008) describe the key role played by orography in anchoring the highly efficient precipitation systems and so increasing the predictability of the location of these events. On the contrary, Cohuet et al. (2011) performed experiments with the 4th October 2007 squall line over Mallorca and concluded that the numerical prediction of the event is extremely challenging due to the high sensitivity of the mesoscale convective system to the initiation phase, which occurred over the sea. In particular, Cohuet et al. (2011) identified a maritime convergence zone over the Alboran Sea during the first hours of 4th October as a determinant precursing structure for the successful simulation of the severe episode. Their finding exemplifies common scenarios that produce high impact events over the densely populated coastal regions of the Western Mediterranean. Despite Cohuet et al. (2011) managed to produce a reasonably good simulation of this convective event with the Meso-NH model, an operationally oriented application requires taking into account the uncertainties associated with the forecast, and thus the use of an ensemble prediction system with the objective of rendering a reliable and high resolution probabilistic description of the plausible outcomes. Given the large and particular challenges identified to numerically predict this squall line, we hypothesize that the application of a cycling EnKF to produce more accurate analyses has a large potential to translate into a higher confidence in predicting the genesis, development and impacts of the severe convective event, than deterministic forecasts.

The paper is organized as follows: Section 2 presents a brief description of the case based on the available observations; Section 3 describes the model and data assimilation system used in this study, as well as the design of the cycling data assimilation experiment. The effects of assimilating conventional data in the forecast of the squall line are discussed in Section 4. Once the positive impact of the assimilated observations is proved, Section 5 describes the role of terrestrial and oceanic measurements on the simulation of the key aspects that produce the improvement in the EnKF experiments. A factor separation technique is used to isolate the influence of the different types of observations in the assimilation. Section 6 provides the discussions and concluding remarks of this study.

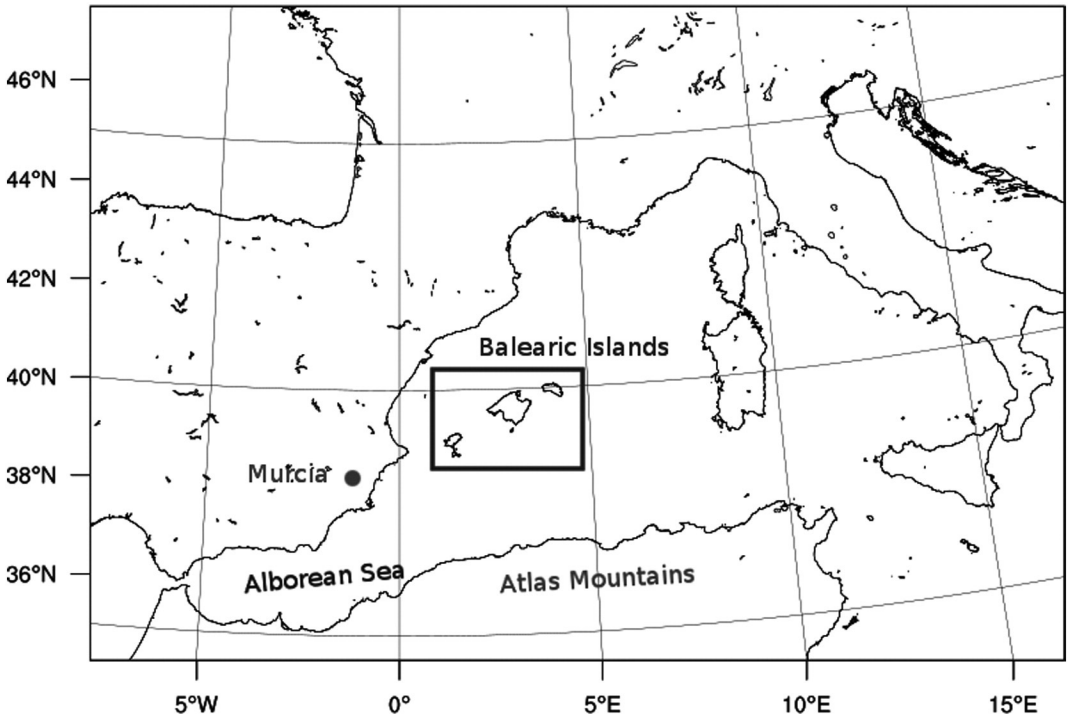

Fig. 1. Numerical domain used in all experiments.

2. The squall line event

On 4th October 2007 a squall line hit the island of Eivissa at 1400 UTC, then the soutwestern coasts of the island of Mallorca at 1530 UTC and continued north-northeastwards, affecting life and property primarily in the southern part of Mallorca and specially in the capital, Palma. The event was characterized by strong gusty winds of about 50 m s^{-1}, torrential rain up to 100 mm h^{-1}, and a greenish tone, characteristic of deep severe convection (Gallagher et al., 1996), was observed as the storm approached the island (Ramis et al., 2009). Furthermore, its intense electric activity, with 160 lightning strikes registered from 1540 UTC to 1550 UTC, provides a good depiction of the thunderstorm track, that initiated offshore Murcia and moved towards the north–east (Fig. 3a). The system matured and reached precipitation rates exceeding the 20 mm h^{-1} during the morning, as registered in raingauges over Mallorca. The AEMET post-storm damage survey indicated the formation of at least three F1–F2 tornadoes embedded in the system.

Infrared Meteosat Second Generation 2 images for that morning (Fig. 3b) show a train of mesoscale convective systems (MCSs) traveling northeast offshore the Mediterranean Iberian coast, from the Alboran Sea to north of the Balearic Islands. The southernmost MCS (MCS3) initiated over the Alboran Sea and progressively became organized until it reached the Balearic Islands (Fig. 3c).

The 1457 UTC image (Fig. 3d) shows the overshooting tops of the thunderstorm, reaching the 200 K cloud top temperatures and revealing an associated anvil area that covered the entire Balearic Channel. Estimated hourly precipitation fields from the composite reflectivities of the AEMET radar network provide a high temporal frequency indication of the location and structure of the thunderstorm initiated at about 0900 UTC (Fig. 4). Despite the Balearics did not have an AEMET radar at that time, the Valencia radar scanned the storm at high elevations and yet clearly depicts the linear organization of the convective system approaching Mallorca (Fig. 3c). As the squall line crossed the mountains that lay along the northwestern coast of Mallorca, the system temporarily lost its linear structure but it eventually reorganized over the sea at about 1700 UTC, moving then to the north. Finally, the system decayed over the gulf of Lyon at about 2000 UTC.

The synoptic situation in which this convective episode unfolded was dominated by a cold upper-level cut-off low over the Iberian Peninsula, and a negatively tilted ridge over Corsica and Sardinia (Fig. 5a). The associated southwesterly difluent flow over the region favoured the synoptic uplift in which the aforementioned train of MCSs formed that morning. At low levels, the cyclonic system located north of the Atlas mountains produced easterly winds that were intensified by the anticyclone located over central Italy, bringing warm and moist advection westwards (Fig. 5b). This easterly low-level flow impinged upon the drier and colder airmass present over mainland Spain, generating an active convergence zone that provided the lifting mechanism for the initial convective cells, as shown by Cohuet et al. (2011). The MCSs observed that day moved along the corridor set by the low-level thermodynamical boundary and the upper-level difluent zone. The interaction of the easterly humid flows with the Mediterranean Spanish coast with the orography is known as a frequent triggering mechanism for heavy precipitation events (Romero et al., 2000; Jansa et al., 2001; Homar et al., 2002). Romero et al. (2014) investigate another example of a maritime squall line initiated to the northwest of the Balearic Islands, along a convergence line also formed under the influence of cyclonic easterly flow. This kind of severe convective system, triggered from pure dynamical mechanisms over maritime surfaces, represents a difficult simulation challenge that limits its predictability, causing substantial socioeconomic impact in the Mediterranean densely populated coastal lands.

3. Numerical tools and experimental set-up

The initialization of mesoscale numerical weather prediction models directly with global coarser resolution fields hinders the successful numerical prediction of events such as the 4th October 2007. Cohuet et al. (2011) unequivocally proved the inability of standard mesoscale set-ups (i.e. non-incorporation of observations) to adequately simulate the evolution of this squall line unless new pieces of information were added to the initial global analyses fields. We explore the use of data assimilation (DA) techniques to ameliorate the numerical forecasts of these events, under the assumption that observations in the region can be efficiently used by means of DA techniques, even at a distance from the measurements.

3.1. Ensemble Kalman Filter

Data assimilation algorithms merge observations with first guess fields in an attempt to distill a more accurate representation of the state of the atmosphere given all available pieces of information (Kistler et al., 2001; Uppala et al., 2005). We use the Data Assimilation Research Testbed (DART, lanai version) software framework. It is a community facility for ensemble data assimilation developed and maintained by the Data Assimilation Research Section at the National Center for Atmospheric Research. It provides DA tools and can be customized to support efficient operational DA applications (Anderson et al., 2009). DART can use different types of assimilation algorithms such as: Ensemble Adjustment Kalman Filter (Anderson, 2001), Ensemble Kalman Filter (Burgers et al., 1998) and a 1D imbedded particle filter (Van Leeuwen, 2010), amongst others. Here, we explore the potential of the EnKF algorithm, a linear and recursive estimator that produces unbiased minimum variance estimates, in a least square sense, of the atmospheric state (Kalman, 1960; Kalman and Bucy, 1961). The observations of the Kalman filter equations are sorted into batches that are assimilated sequentially. As more batches of observations are assimilated, the background state of the ensemble is updated and eventually become the analyses field (Houtekamer and Mitchell, 1998a). The algorithm is stochastic in the sense that it uses a random number generator producing draws from the observation likelihood distribution (Anderson et al., 2009). EnKF estimates the background error covariance matrix from the statistical properties of an ensemble of forecasts, which is a considerably simpler method compared to other assimilation approaches. Although not strictly necessary, when EnKF is implemented as a cycling DA system, in which an update step where observations are assimilated, is followed by a forecast step in which the distribution of atmospheric states, and thus also the error covariance matrix, are evolved in time. Repeatedly estimating the error covariances in cycles from the ensemble of high resolution forecasts has a clear impact on the quality of the resulting ensemble of analyses, which in turn improve the accuracy of the associated forecasts.

EnKF has been widely applied and examined since it was first introduced in meteorology by Evensen (1994), showing substantial improvements in the prediction of subsynoptic phenomena. Some examples of this studies are found in: Snyder and Zhang (2003) and Zhang et al. (2004), which assimilate synthetic radar data; Dowell et al. (2004) in which real radar observations were assimilated for a tornadic supercell thunderstorm; Marquis et al. (2014), which proved the value of assimilating high-resolution Doppler radar velocities and in situ surface observations into a simulated convective storm, also performed by Sippel et al. (2013) and Tanamachi et al. (2013).

3.2. Forecast model

The numerical model used in all experiments presented in this paper is the WRF-ARW mesoscale model version 3.4. We defined a numerical domain that covers the area of interest over the Western Mediterranean with a 16 km horizontal grid size (Fig. 1). Similar setups have been successfully implemented over the central plains in the US in order to characterize the mesoscale environment in which severe weather outbreaks unfold (Fujita et al., 2007; Yussouf et al., 2013; Wheatley et al., 2014). In order to increase the number of error sources accounted for in the

experimental probabilistic forecasting system, we use multiple parameterized physics configurations amongst the ensemble members. We use two convective schemes: Kain–Fritsch and the new simplified Arakawa–Schubert scheme. The Kain–Fritsch uses an updated cloud model with respect to Kain and Fritsch (1990) that performs the entrainment and detrainment as a function of the buoyancy characteristics of various mixtures of clear and cloudy air. The new Arakawa–Schubert parametrization features a new mass-flux scheme with deep and shallow convection, along with momentum transport. We also add diversity to the ensemble by using multiple planetary boundary layer (PBL) schemes. PBL is a determinant factor in accurately simulating mesoscale weather phenomena (Pielke and Mahrer, 1975; Ogura and Chen, 1977; Ulanski and Garstang, 1978) due to the critical role heat and momentum fluxes play in the unfold of severe phenomena. Li and Pu (2008) showed that PBL schemes play almost the same role as cloud-microphysics schemes in accurately forecasting hurricane intensity. Four PBL schemes are used: Yonsei University (YSU) (Hong et al., 2006), Mellor-Yamada-Janjic (MYJ) (Janjic, 1990), Asymmetric Convective Model (ACM2) (Pleim, 2007) and Mellor-Yamada Nakanishi and Niino Level 2.5 (MYNN2) (Nakanishi and Niino, 2004). Finally, given the specific geographical characteristics of the Western Mediterranean basin and its surroundings, the variability of aerosol concentration in the various air masses that invade the region is clearly underestimated by standard tabulated aerosol parameters in the microphysical scheme. Saharan, continental central European, Atlantic or purely Mediterranean air masses have radically different aerosol characteristics (Clarke et al., 1997), being very influential on the moist physics processes in the Mediterranean region. To account for this variability and cope with the errors of using tabulated cloud condensation nuclei (CCN) data, we prescribe 3 levels of CCN (see Table 1).

3.3. EnKF experimental design

The cycling EnKF and the subsequent forecast phases are adapted to the problem in hand. To begin, an initial first guess of the probability distribution of atmospheric states valid hours before the beginning of the forecast phase is needed. We use a 24-members ensemble extracted from the operational European Center for Medium Range Weather Forecasts (ECMWF) global Ensemble Predictions System (EPS) which run at a resolution of T399L62. We choose the 24 members with the largest diversity across the numerical domain (Fig. 1) using a method based on Principal Components Analysis and k-means clustering applied over the original 50 members of the ECMWF EPS (Garcies and Homar, 2009). We use 500 hPa geopotential and 850 hPa temperature fields. In the end, the selected members have the largest differences amongst the 50 in terms of the clustering fields over the domain. This initial first guess is thus composed by 24 members off the ECMWF EPS initial state (i.e. perturbed analyses), valid at 00 UTC 4th October 2007. The first EnKF update step is performed and also valid at this time. We use observations archived at the Meteorological Assimilation Data Ingest System (MADIS) maintained by the National Weather Service of the National Oceanic and Atmospheric Administration. In particular, we use radiosonde, METAR, marine, and ACARs data (Fig. 2 and Table 2). Admittedly, first assimilation cycle is clearly suboptimal because the first guess fields have an effective resolution of roughly 50 km (T399), and thus the error covariance matrix used is not yet adjusted to the 16 km potential resolution of the numerical fields. The resulting 24 members from the first update step are integrated forward for one hour in the forecast step. At 0100 UTC a new update step is performed and the process is repeated until the last update step at 0600 UTC (i.e. 1-hour cycles for 6 h (Houtekamer et al., 2005 ; Fujita et al., 2007)). The number and type of observations vary significantly between cycles (Table 2). As expected, the largest number of available observations is found at 00 UTC and 06 UTC, with 883 and 720 respectively, although at all cycles a minimum of 380 observations are assimilated. METAR observations are systematically the most numerous over the entire assimilation window, varying from 300 to more than 550 measurements, and marine records are the least numerous, with 191 observations over the entire window. Although the variability of observations is evident between cycles, the overall assimilated dataset covers adequately the area under study (Fig. 2). The resulting analysis fields become the initial conditions for a 24-members ensemble forecast that spans for 18 h, until 00 UTC 5th October 2007.

Table 1
Multiphysics configurations used in the 24-member ensembles.

PBL	CCN	Cumulus
YSU	*1.50E + 09*	*Kain-Fritsch*
MYJ	*1.00E + 09*	*New Simplified Arakawa Shubert*
ACM2	*5.00E + 08*	
MYNN2		

On account of the moderate size of this EPS system, covariances tend to be underrepresented and masked by artificial correlations, resulting in a suboptimal analyses (Hacker et al., 2007). One of the most prevalent methods used to reduce the negative impact of these kinds of errors is to use localization (Houtekamer and Mitchell, 1998b). Typically, localization is performed through a distance weighting-covariance function that becomes zero exceeding the cutoff length (Sobash and Stensrud, 2013). To mitigate errors due to limited ensemble size, horizontal and vertical covariance localization is implemented (Mitchell et al., 2002). In this study, we have used as a weighting-covariance function an approximation of a Gaussian function (Gaspari and Cohn, 1999), with 300 km horizontal cutoff parameter and 4 km for the vertical.

Another essential aspect to consider when dealing with reduced ensemble sizes and because of model and sampling error is the inflation factor (Anderson and Anderson, 1999). In such situation, filter algorithms as EnKF, tend to collapse towards a single solution, leading to insufficient dispersion within the ensemble (Furrer and Bengtsson, 2007). State-space inflation method consists in increasing the spread of the ensemble to avoid convergence and collapse problems. In this work, we use a time-evolving inflation value, characterized by a Gaussian distribution, where the mean is the initial value of the inflation and the standard deviation controls how rapidly the inflation evolves in time. Large values of the standard deviation values mean that the inflation will vary more quickly with time. We use as initial inflation value 1 and 0.6 to the standard deviation. The inflation factor adapts to the various spatial and temporal observational densities provided to the system.

3.4. Non-assimilation ensemble design

In order to analyse the added value of using an EnKF cycling assimilation scheme in the numerical forecast of this maritime severe episode, we design two additional ensemble systems with no assimilated observations. These are built by directly initializing the mesoscale ensemble of WRF runs with ECMWF EPS members. The first experiment (NOA00) uses the same 24 ECMWF EPS members selected in the initial update phase of the EnKF experiment (i.e. initial perturbed global analyses of the 00 UTC ECMWF EPS as initial conditions and the corresponding forecasts as boundary conditions). The forecast runs for 24 h, until 00 UTC 5th October. The second experiment (NOA06) is identical to NOA00 except for the initiation time, which is set to 6 h later. For this experiment, the initial fields are 6 h forecasts from the 00 UTC cycle of the ECMWF global EPS, using the same set of global members. Contrary to the NOA06, the 6 h time shift in the NOA00 is expected to allow for a spinup period before the initiation of convection. The forecasts for the NOA06 experiment spans for 18 h and also use the corresponding forecasts from the global ensemble as boundary fields. Both experiments use the very same numerical configuration as the EnKF ensemble.

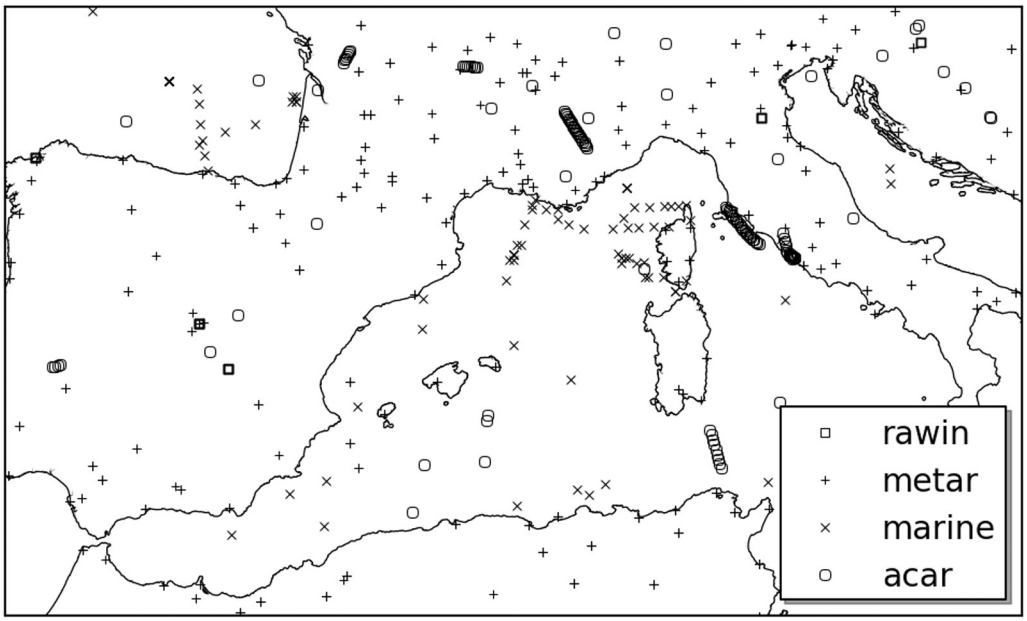

Fig. 2. Spatial-distribution of MADIS observations assimilated on 4th October 2007 between 00–06 UTC.

4. Results

Representing the initiation, organization and evolution of convection in maritime events is a challenge for numerical weather prediction systems, which have to accurately simulate both synoptic and mesoscale structures to render useful predictions. We compare the performance of EnKF, NOA00 and NOA06 ensembles presented above, focusing on their ability to predict the hazard associated with the 4th October event.

4.1. Probability of severe

We design a product (Probability of Severe (PoS)) to assess synthetically the severe convective activity generated by each ensemble. An event is defined as either hourly precipitation accumulations over 30 mm or 925 hPa windspeed exceeding 80 km h^{-1} for each gridpoint and ensemble member. The instantaneous probability of severe is a grid-point value calculated as the frequency amongst ensemble members of an event occurring in that gridbox. The probability of severe over a certain period is computed recursively using the standard additive law of probability combining instantaneous probabilities by pairs:

$$P_{t1,t2} = P_{t1} + P_{t2} - P_{t1 \cap t2} \quad (1)$$

In our case and for all 3 experiments, the PoS is computed over the 06–18 UTC interval. This product provides a quick glimpse of the areas threatened by heavy rain rates or strong winds as predicted by each experiment (Fig. 6). NOA00 produces four distinct areas of probable convective activity: one over the Moroccan coast, which was persistently affected by deep convection during the morning and early afternoon of 4th October, as clearly identified over the MSG-2 images; one north of the eastern Pyrenees, which was also affected by convection, although with lower intensity. The northeastern coastal region of the Iberian Peninsula is also highlighted because many NOA00 ensemble members develop intense convection when the easterly low-level flow impinges the eastern edge of the Iberian cold air mass. The MCS3 system (Fig. 3b) produced a left splitter storm, which moved northwards and affected the northeastern coast of Spain during the late morning hours. The convection predicted by the ensemble over the fourth area resembles the storm that affected Mallorca that afternoon. Only a few NOA00 members trigger convection over the Alboran Sea, with even less developing intense convection and reaching the Balearics. The remaining members neither show a linear organization of the storm nor follow the observed northeastern path towards Mallorca. This renders only minor PoS offshore Murcia and probabilities below 0.1 over the actual squall-line path. Initializing the ensemble 6 h later does not produce substantial changes in the guidance provided as for severe effects of convection is concerned. Although the detailed evolution of the convective system in individual ensemble members is diverse, the distribution of plausible convective activity rendered by NOA06 is, in practice, analogous to the NOA00 results. The most notable improvement in NOA06 is the increased number of members triggering storms over the Alboran Sea and being steered north, along the Balearic Channel, to the west of the observed squall-line. These results show that neither the allowance for some spinup time in NOA00 nor the shorter lead-time conceded to the NOA06 experiment render any significant difference in the guidance for the prediction of severe convection. The simple downscaling of the global ECMWF-EPS system does not suffice to adequately provide the mesoscale environment in which the linear convective system triggered, intensified, organized and evolved northeast from the Alboran Sea. This fully agrees with the conclusions reached by Cohuet et al. (2011).

The value of including new sources of information by assimilating in-situ observations is evident from the EnKF experiment results. This experiment shows high probability of intense convective activity over the Alboran Sea, resulting mostly from convection triggered during the first hours of simulation, in good agreement with the initiation of storms over the area observed in the MSG-2 images (Fig. 3). This result supports the crucial contribution of the assimilated observations on the configuration of the environment in which the linear convective system that affected the Balearics initiated. A majority of ensemble members trigger convection over that area during the morning, and half of them

Table 2
Number of observations per type for each assimilation cycle.

obs_type|Hours-(UTC)	*0*	*1*	*2*	*3*	*4*	*5*	*6*	*Total*
Marine	*43*	*18*	*24*	*34*	*22*	*12*	*38*	*191*
Acar	*4*	*4*	*30*	*22*	*0*	*83*	*114*	*257*
Metar	*375*	*345*	*335*	*375*	*421*	*474*	*568*	*2893*
Rawin	*461*	*57*	*0*	*0*	*0*	*0*	*0*	*518*
Total	*883*	*424*	*389*	*431*	*443*	*569*	*720*	

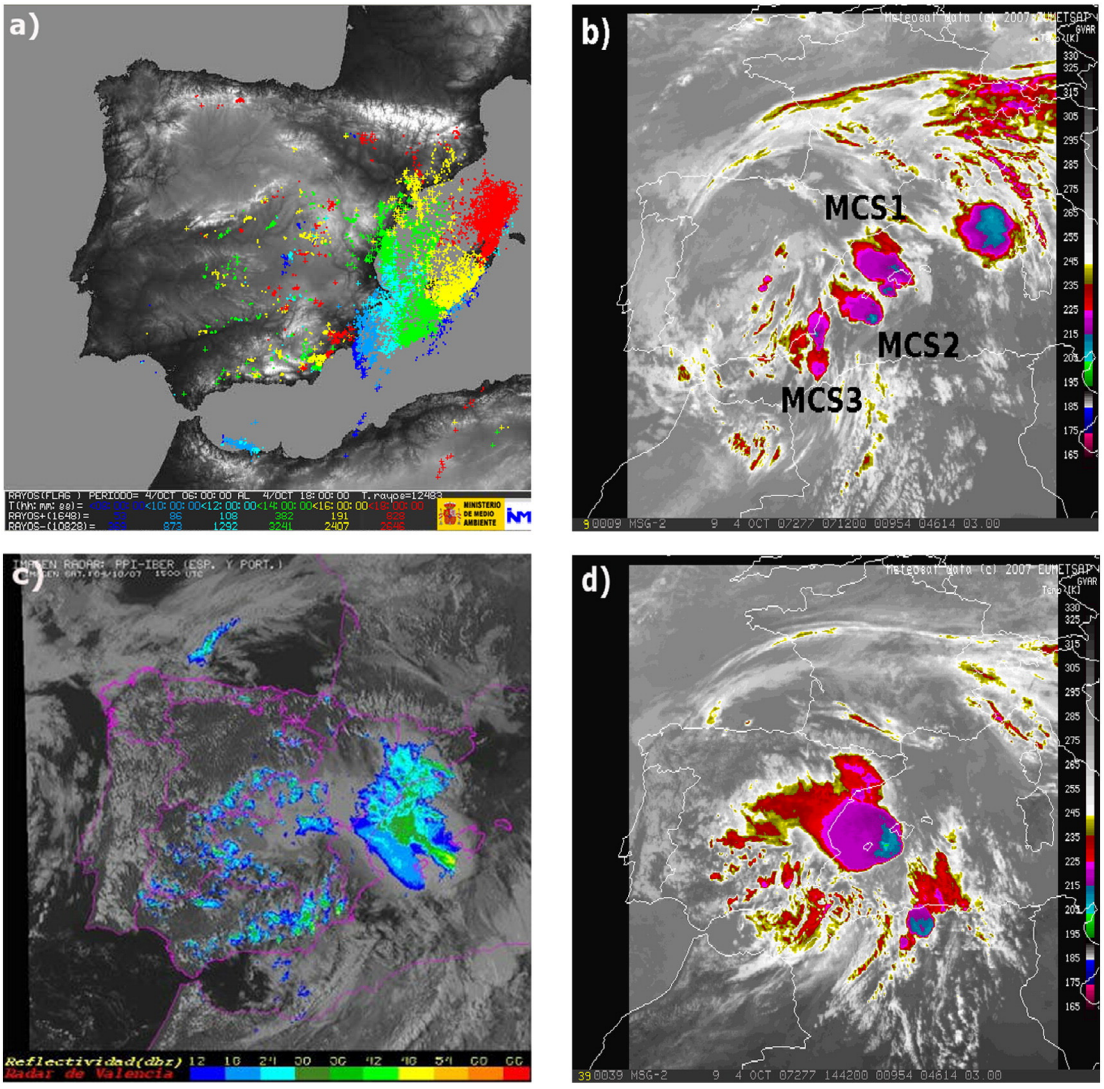

Fig. 3. (a) Lightning strokes between 0800 UTC and 1800 UTC. Colors indicate time interval of measurement, as indicated in the table at the bottom of the panel. IR MSG-2 brightness temperature according to the right-hand scale on 4th October 2007 at 0712 UTC (b) and 1500 UTC (d). (c) Radar composite image at 1500 UTC.

show the system evolving remarkably close to the observed storm. This mixture of convective evolutions simulated by the ensemble renders a PoS that provides a very indicative outlook of the areas under severe weather threat for that day. In addition, EnKF reduces the PoS over the northeastern Iberian Peninsula with respect to the no-assimilation experiments, in agreement with the actual impact on that area (Fig. 3). On the contrary, the system over the Moroccan coast is well predicted by all three experiments, and the presence of southwesterly (terrestrial) flow steering the convective cells over that area, together with the orographic anchoring of this intense system explains its high predictable character.

4.2. Environment characterization

Differences detected between experiments can be tracked back to the environment simulated by each member in which convection occurred. According to the standard squall-line conceptual model (Markowski and Richardson, 2011), three ingredients (Doswell et al., 1996) are required for their formation: low-level wind shear, convective instability and a triggering mechanism. Each ensemble member of all three experiments show high values of low-level wind shear during the morning and afternoon of 4th October along the warm air southerly air intrusion, east of the Iberian Mediterranean coast. All members produce 0-3 km wind shear exceeding 20 m s^{-1} and thus differences in PoS cannot be attributed to this dynamical environmental preconditioning factor. Regarding buoyancy, the environment was very supportive for convection development. High values of conditional instability are simulated in most members of all three experiments throughout the western part of the Western Mediterranean, along the Iberian coast (Fig. 7). The field of combined probabilities of CAPE of the most unstable layer (mCAPE) exceeding 400 J kg^{-1} and CIN below 150 J kg^{-1} does not reveal substantial differences amongst EnKF, NOA00 and NOA06 offshore southeastern Iberian Peninsula. When analysed in detail, the EnKF shows higher confidence in the presence of conditional instability along the path of the observed convective systems than the experiments with no assimilation. A substantial difference is observed over the Tyrrhenian Sea, where EnKF shows a distinct signal for a favourable convective thermodynamical environment. This disparity originates mainly from the assimilation of ACAR measures, which produce the cooling of two layers: an elevated layer between 900–750 hPa (which reduces CIN) and a mid-levels layer between 600–500 hPa (which increases CAPE). However, regarding the area of interest, all three experiments simulate environments with moderate values of low-

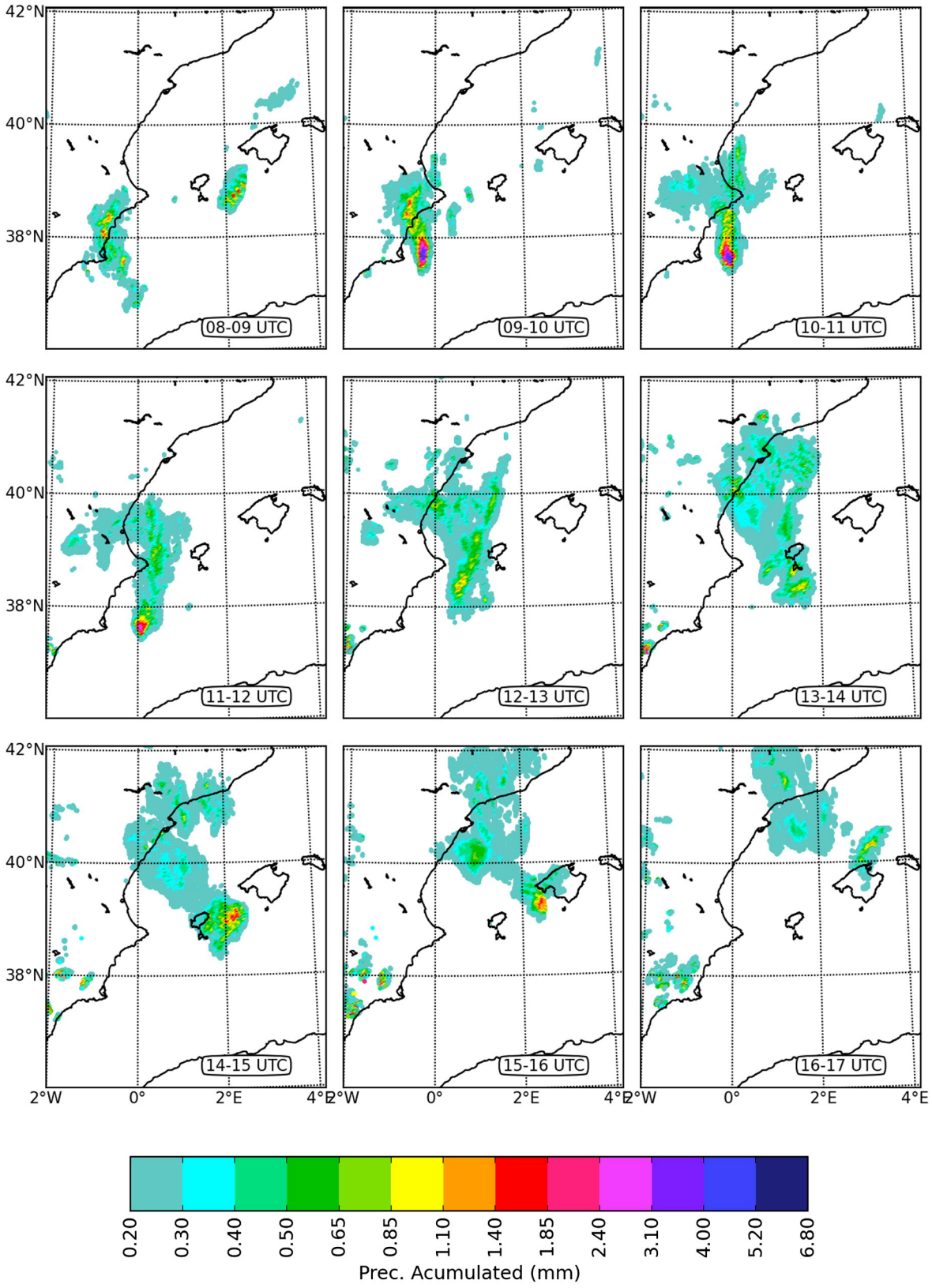

Fig. 4. Acumulated hourly precipitation composite from the AEMET radar network for the period 0900 to 1700 UTC on 4th October 2007.

level shear and sufficient conditional instability for the severe convective episode to unfold.

Conversely, remarkable differences are identifiable in the mesoscale thermodynamical and dynamical low-level simulated environment between EnKF and NOA00. The analyses obtained from the 00 and 06 UTC assimilation cycles depict a warm front offshore Murcia penetrating over a colder air mass and the initiation of a weak convergence area (Fig. 8b and d), allegedly linked to the triggering of the convective cells

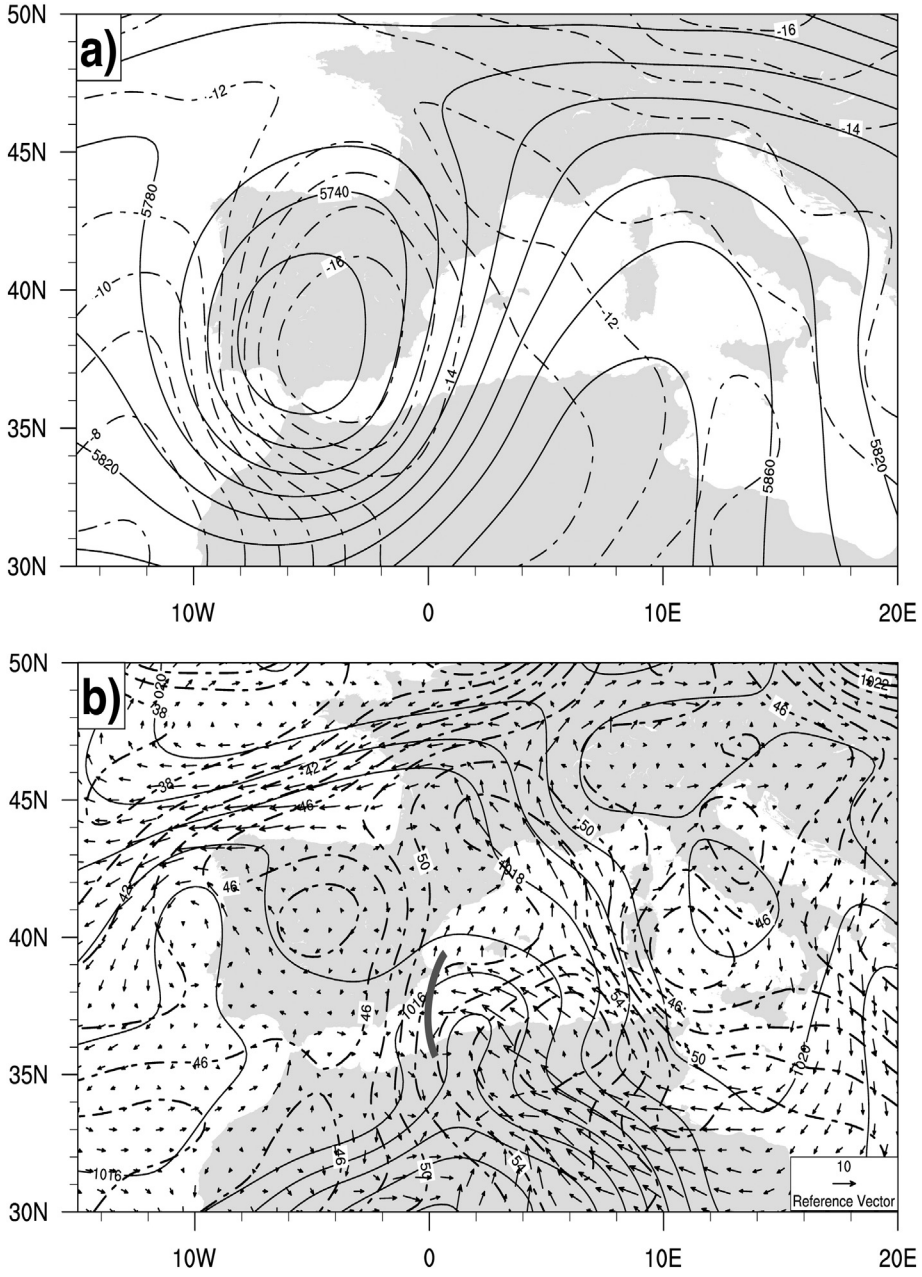

Fig. 5. ECMWF analyses at 06 UTC 4th October 2007 of (a) 500 hPa geopotential height (solid lines, mgp) and temperature (shaded lines, °C); and (b) 925 hPa equivalent potential temperature (shaded lines, °C), wind (vectors, m s^{-1}) and sea level pressure (solid lines, hPa). The thick line highlights the convergence zone referred to in the text.

that led to the squall line formation. The NOA00 fields show a weaker thermal perturbation and no indication of the convergence zone is traceable neither at the initial time (00 UTC, Fig. 8a) nor after 6 h of simulation (Fig. 8c). Certainly, these flow patterns produced by the EnKF system become determinant for the successful prediction of the probabilities of severe weather observed in Fig. 6. Indeed, a key ingredient for the correct simulation of this squall line event was already hypothesized by Cohuet et al. (2011), which pointed at a convergence line at low levels offshore Murcia as the determining factor for the useful prediction of the event. They proved the benefits of nudging a synthetic convergence line over the Alboran Sea on the first hours of 4th October. Even though the divergence field becomes notably noisy at these resolutions, a clear signal of the convergence zone is identifiable in the EnKF output fields. For the sake of synthesis and with the aim of showing the ensemble divergence results without smoothing out any relevant signal, we determine the most likely sign and probability level of the low-level divergence field (Fig. 9). In order to perform a fair comparison in terms of timing, and since we are analysing the effect of low-level convergence on the triggering of convection, we focus on the initiation time of the first convective cells in each experiment individually (see Fig. 9 caption for details). The EnKF ensemble provides an accurate representation of the low-level convergence, shown as a large region with mostly convergent members overlapped with incipient precipitation values. With time, these convective systems grow and move northeast, towards Mallorca. On the contrary, both the NOA00 and NOA06 show only a marginal number of convergent areas within the ensemble around the initiation region (Fig. 9). Indeed, a comparison of the low-level convergence fields at the corresponding simulated initiation times amongst the experiments clearly reveal the origin of the differences between the PoS fields rendered by the three ensembles (Fig. 10).

Therefore, the assimilation of available observational data during the first six hours of 4th October does not have a significant impact on the

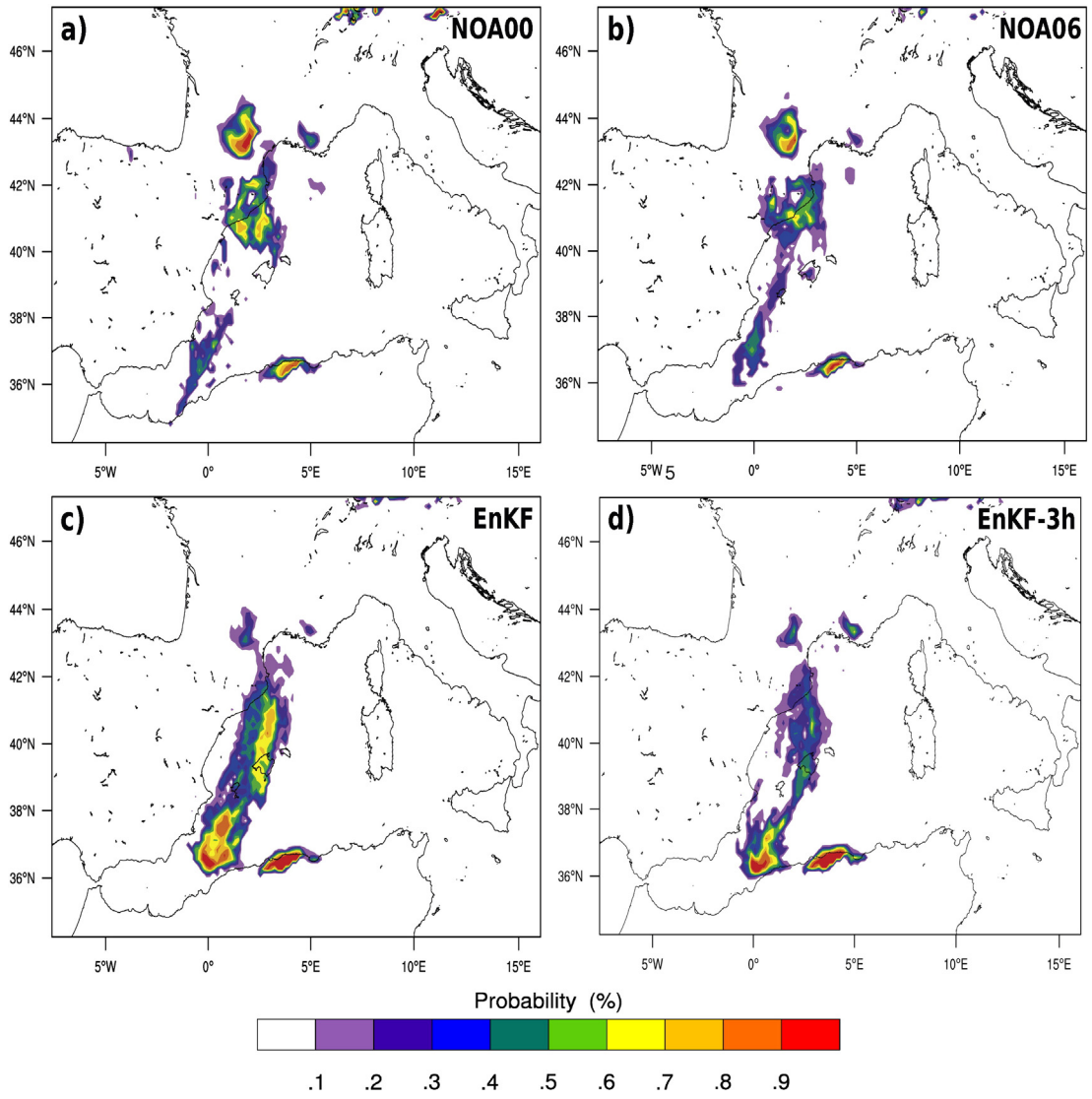

Fig. 6. Probability of Severe over the 06–18 UTC period for (a) NOA00, (b) NOA06, (c) EnKF and (d) EnKF-3h experiments.

simulated thermodynamical environment of the westernmost Western Mediterranean, but the EnKF system accurately represents the location and time of the low-level convergence zone responsible for the initiation of the convective system that later evolved to the northeast in the highly convectively unstable and high shear environment, ultimately acquiring the linear shape and severe intensity.

4.3. PoS verification

A quantitative verification of the PoS field allows to synthetically determine the impact of the assimilation of observations. We use lightning data as a reliable proxy for severe weather, with the notable advantage of being spatially homogeneous and cover maritime zones. As the goal of this analysis is to verify a probabilistic field, we employ kernel density estimation (KDE, Bowman and Azzalini (1997)), which estimates the probability density function of the lightning (e.g. severe) location random variable from the collection of available samples (i.e. lightning locations, (Fig. 3a)). The kernel function implemented for each lightning detection is a 2D-Gaussian with a bandwidth $h = \sigma$. The bandwith quantifies the uncertainty scale of the occurrence of the lightning, and is set to $h = 17$ km, which is within the meso β scale (Fujita, 1981), typical length scale for convective cells. Making use of the additive law of probability to sum up the contribution of each lightning record, we compute the integrated 06–18 UTC probability density function of lightning (PoL). The skill of the various PoS fields (see Table 3), is verified against PoL by means of areas under ROC curves (AUC, (Stanski et al., 1989) and (Schwartz et al., 2010)). False alarm rates (FAR) for all probability forecast thresholds are remarkably low, due to the high density of lightnings recorded for these events (Fig. 3a) and the common bias to underpredict severe convective activity in all three experiments. However, EnKF Hit Rates (HR) are superior to the NOA00 and NOA06, yielding larger AUC values (Fig. 11a). EnKF shows HR near 0.5 for

Table 3
Observation type assimilated in each experiment performed.

Experiments	Metars	Marine	Acars	Rawin
EnKF	1	1	1	1
EnKF73h	1	1	1	1
NOA00	0	0	0	0
NOA06	0	0	0	0
UPP	0	0	1	1
SFC	1	1	0	0
NM	1	0	1	1
M	0	1	0	0
NWM	1 (except wind metars)	1	1	1
ACARS	0	0	1	0

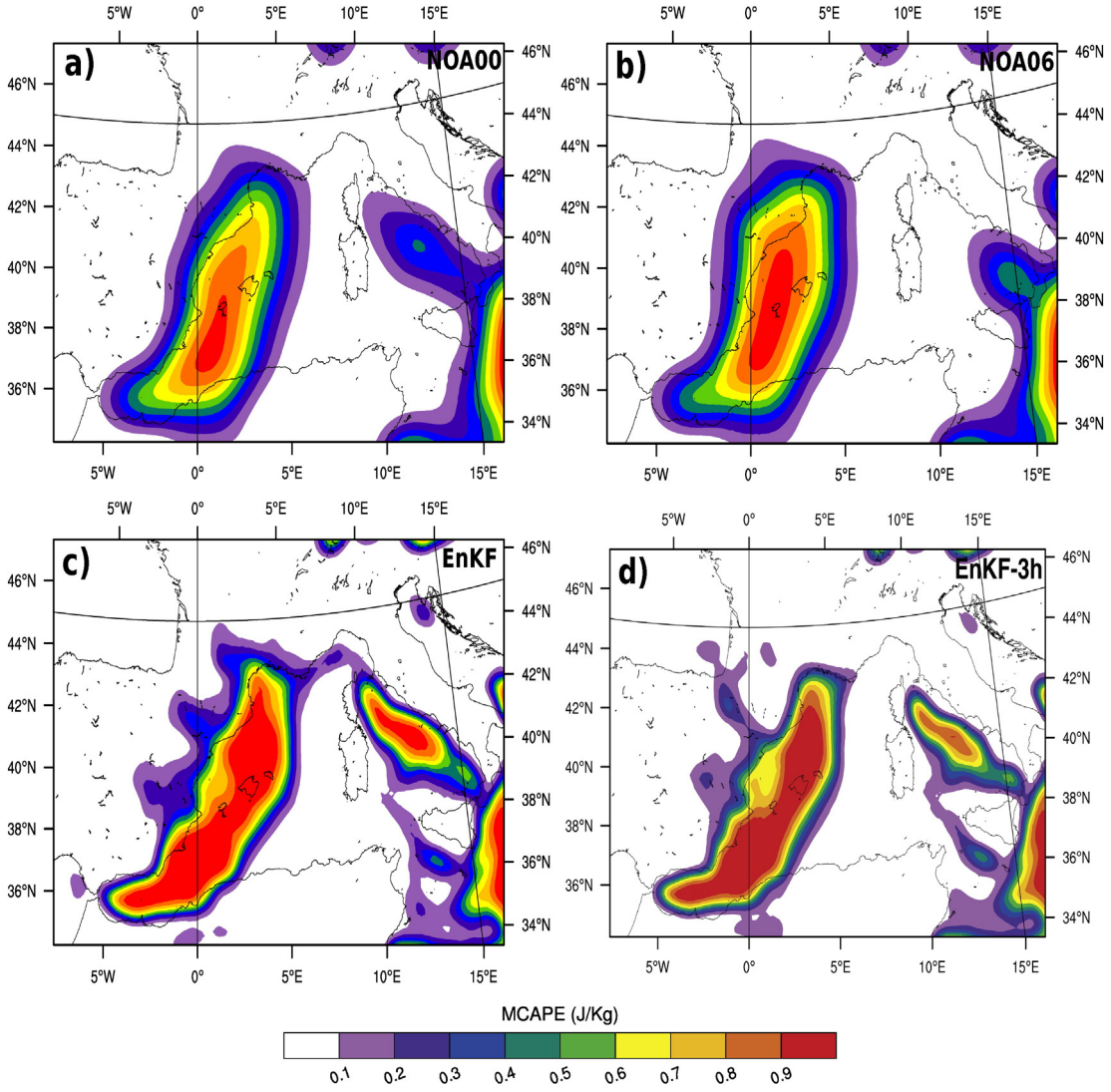

Fig. 7. Probability of most unstable layer mCAPE exceeding 400 J kg^{-1} and CIN below 150 J kg^{-1} for (a) NOA00, (b) NOA06, (c) EnKF and (d) EnKF-3h experiments.

predictions of notable probabilities of severe (PoS > 10%), which is remarkably high for the prediction of extremes. NOA06 and NOA00 render lower HR, with NOA06 producing a better PoS field due to a slightly better handling of the convergence line over the Alboran Sea responsible for the initiation of the convective systems. These results quantify the added value of assimilating conventional observations for the prediction of maritime severe convective systems near coastal areas, and encourage analysing further the causes of such definite improvement.

5. Attribution to observation type and frequency

Given the positive impact observations have in the simulation of the dynamical context in which the convection initiated, we explore the role of changing the frequency of assimilations, as well as the role of various observation types in that gain (see Table 3 for a list of experiments). In order to better analyse the transition from no assimilation to 1-hourly updates, we perform an intermediate experiment in which observations are ingested at 3 h intervals (namely 00, 03 and 06 UTC, EnKF-3h), using a ±30 minute assimilation window (Fig. 6d). PoS values have been reduced from 60–70% to 40–50% over Mallorca Island, and from 30–40% to 0–10% over Eivissa Island. PoS around the initiation area of the thunderstorm, offshore Murcia, has also been reduced significantly. These changes cannot be attributed to a significant modification of the environmental energetics when 1 h (Fig. 7c) updates are used compared to 3 h (Fig. 7d) or lower frequencies. The probability of adequate CAPE and CIN values for deep convection is not notably changed, reflecting the low temporal variability of these thermodynamical fields at the resolved scales. Allegedly, differences between EnKF and EnKF-3h PoS are again attributable to the low-level convergence area responsible for the triggering of the thunderstorm. The positive impact of 1 h updates in the assimilation cycle with respect to the 3-hourly strategy is shown in terms of AUC values (Fig. 11b). These results reveal the smooth transition in the forecast fields as observational information is gradually added to the system.

Regarding the role of observations types, a first experiment (UPP), in which upper-level observations are assimilated, i.e. radiosonde and ACAR measurements (775 in total), is performed. This experiment contains only information from surface observations contained already in the ECMWF EPS system at 00 UTC and, in a strict sense, also through the boundary conditions. The second experiment SFC is the complementary, in which only surface measurements (a total of 3084 between METAR and marine) are assimilated over the 6 h interval. Given the high sensitivity of the predictability of this event to the accurate representation of the local low-level mesoscale flows, the results from these experiments confirm the higher influence of surface over upper-air observations on the prediction improvement obtained for the EnKF with respect to the non assimilating NOA00 and NOA06 experiments. This

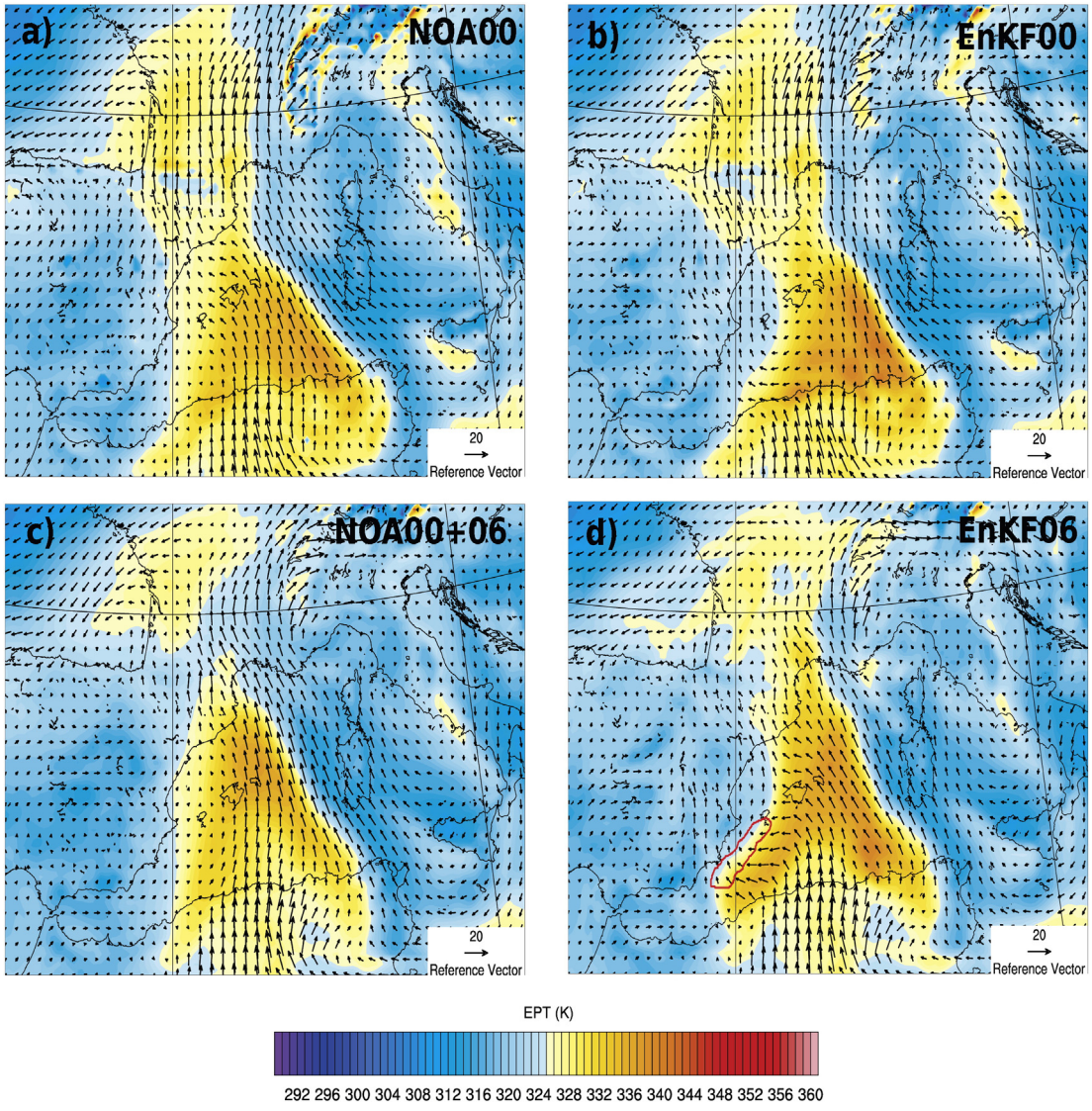

Fig. 8. Ensemble mean equivalent potential temperature (K, shaded) and the wind field (m s^{-1}, vectors) at 925 hPa for the experiments NOA (a and c) and EnKF (b and d). Upper (lower) panels show 00 (06) UTC fields. The red contour in panel (d) highlights the convergence zone discussed in the text (For interpretation of the references to colour in this figure legend, the reader is referred to the web version of this article.).

notable improvement is not necessarily attributable to the higher number of surface observations compared to the upper-air, but to the relevance of the information they provide, which is essential to adequately represent the low-level flow near the convective initiation area. The degradation in PoS obtained by the UPP experiment is not only evident over the initiation area but all along the squall line path (Fig. 12). Conversely, not assimilating upper air measurements, as done in the SFC experiment, has only marginal effects on the distribution of PoS across the threatened area, not modifying significantly the detection of the severe threat. Again, when tracking these differences back to the physical ingredients, a remarkable disagreement is found in the probability of low-level divergence field during the first hours of the day simulated by UPP and SFC (Fig. 13). The assimilation of upper-level data alone does not render the large area of probable convergence south of the Balearics and along the Moroccan coast, which is clearly attributable to the surface observations. However, it is noteworthy that the impact of assimilating surface data, calculated as the difference between EnKF and UPP, (Fig. 13a), generates a nuclei of convergence offshore the Moroccan coast just east of the Greenwich meridian, which enhances the probability of initiation over that area in the full EnKF experiment. On the contrary, the impact of assimilating upper-air measures is negligible (Fig. 13b).

The large influence of surface observations is in good agreement with the hypothesized conceptual model of information being advected from observed regions towards data-void areas. In order to confirm this, we study the distinct effect observations over land and over sea have on the prediction of severe threat. We apply the factors separation technique (Stein and Alpert, 1993) to determine quantitatively the influence of maritime (M) and terrestrial (NM) observations have on the PoS field (Table 3), with the additional benefit of isolating the synergistic effect of both factors on the predictand field. The technique requires 2n simulations, with n the number of factors, which we set to 2: measurements over land and measurements over sea. Once the calculations to isolate each effect are performed, we find that the effect of terrestrial observations is positive in terms of highlighting the severe threat along the observed path of the most active convective cells for the day, and specially the squall line. Land observations contribute specially at intensifying probabilities near the initiation area, south-west of the Western Mediterranean and across an elongated area to the north, that covers the Balearic Islands (Fig. 14). The maritime contribution is much weaker

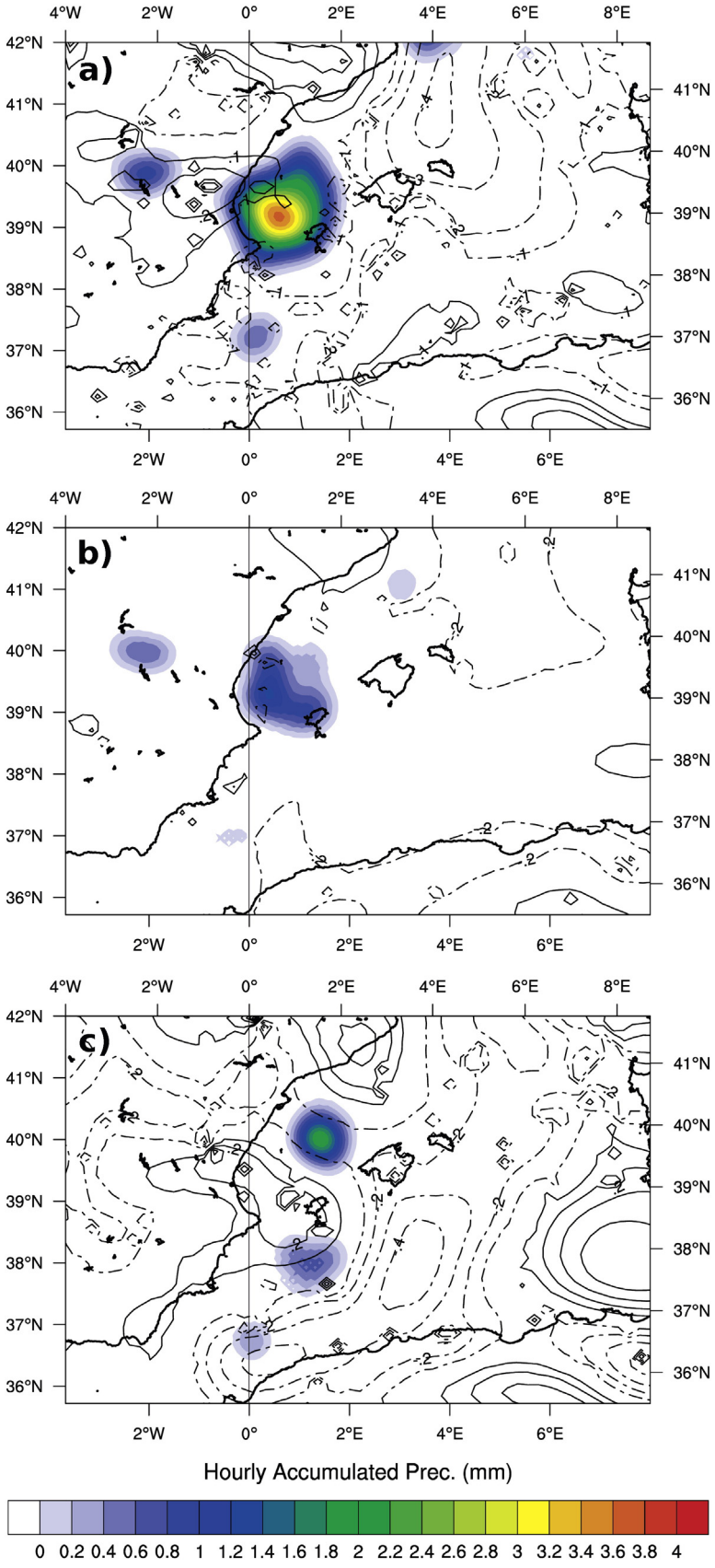

Fig. 9. Probability of divergence (solid line) and convergence (dotted line), and 1h accumulated mean precipitation fields at the MCS3 initiation time for (a) NOA00 experiment at 0400 UTC; b) NOA06 experiment at 0800 UTC and c) EnKF experiment at 0700 UTC). Only the largest convergence or divergence probabilities are plotted in each gridpoint. Absolute values of divergence below $-5 \cdot 10^{-3}$ are not accounted for in the probability calculations. Probabilities are plotted in 0.1 intervals.

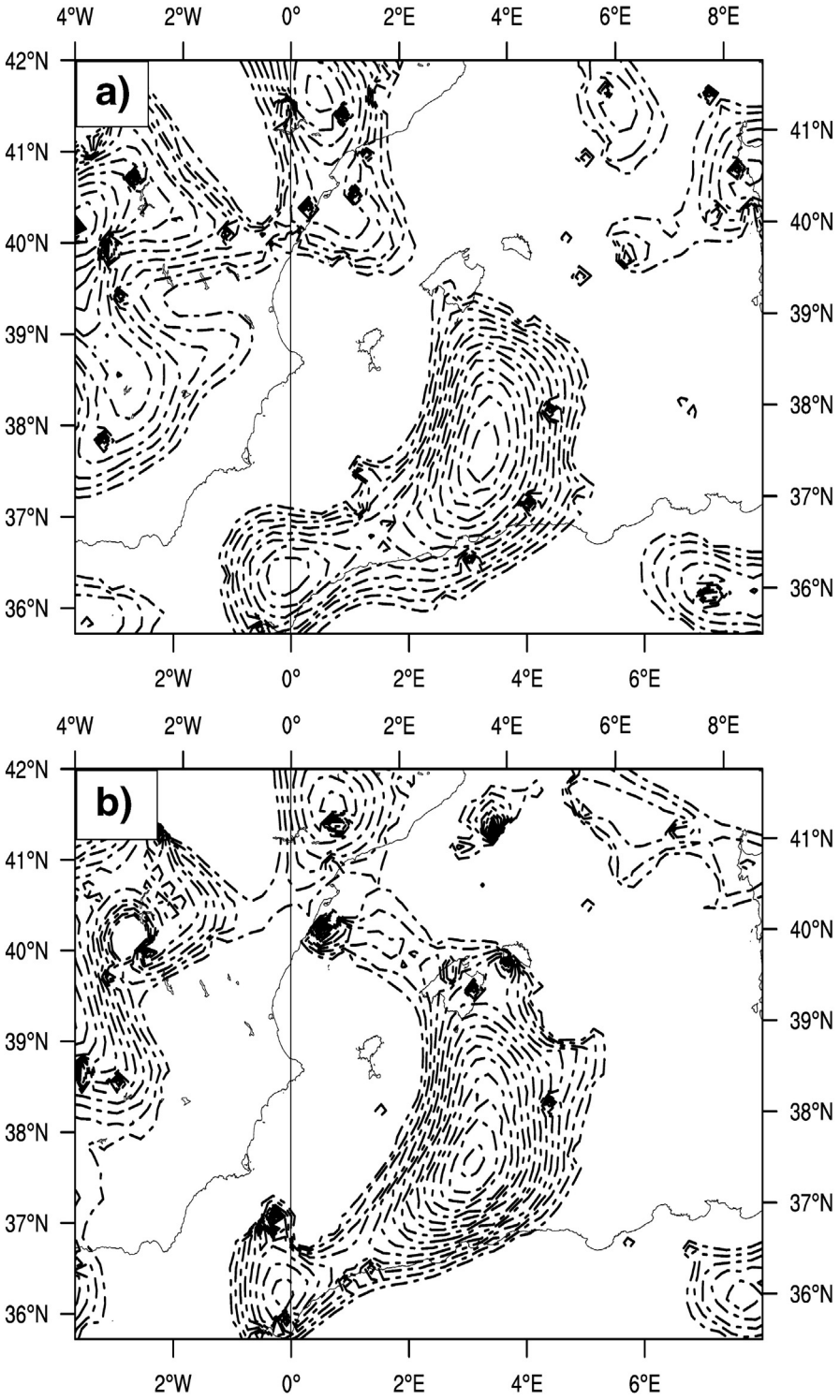

Fig. 10. Difference in probability of convergence between EnKF and a) NOA00 ; b) NOA06 at the corresponding simulated initiation time.

but also contributes to increase the chances of severe phenomena near the observed initiation area and over an area north of the Balearic Islands. The quantitative verification confirms this with AUC values of 0.67 and 0.57 for land and marine observations (Fig. 11b). The effects attributable to the simultaneous use of both measurement types are also interesting, with a general shift of the larger probabilities towards the west, specially at the southern tip of the area under severe weather threat, offshore the Moroccan coast. A common result when applying the factor separation technique is the cancellation of particular features exhibited by the factors or their synergism. In this case, the EnKF does not show significant probabilities of severity for the convective system over southern France, because the positive contribution of the synergism over the area is cancelled by the isolated contribution of maritime measurements.

Surface measurements emerge as relevant sources of valuable information to improve the low-level analyses, including the convergent flow, the simulated convective initiation and the further prediction of the PoS. Brousseau et al. (2014), concluded that assimilation of surface-wind was very valuable for the analyses of low-level wind. Following their results, we performed an experiment excluding wind

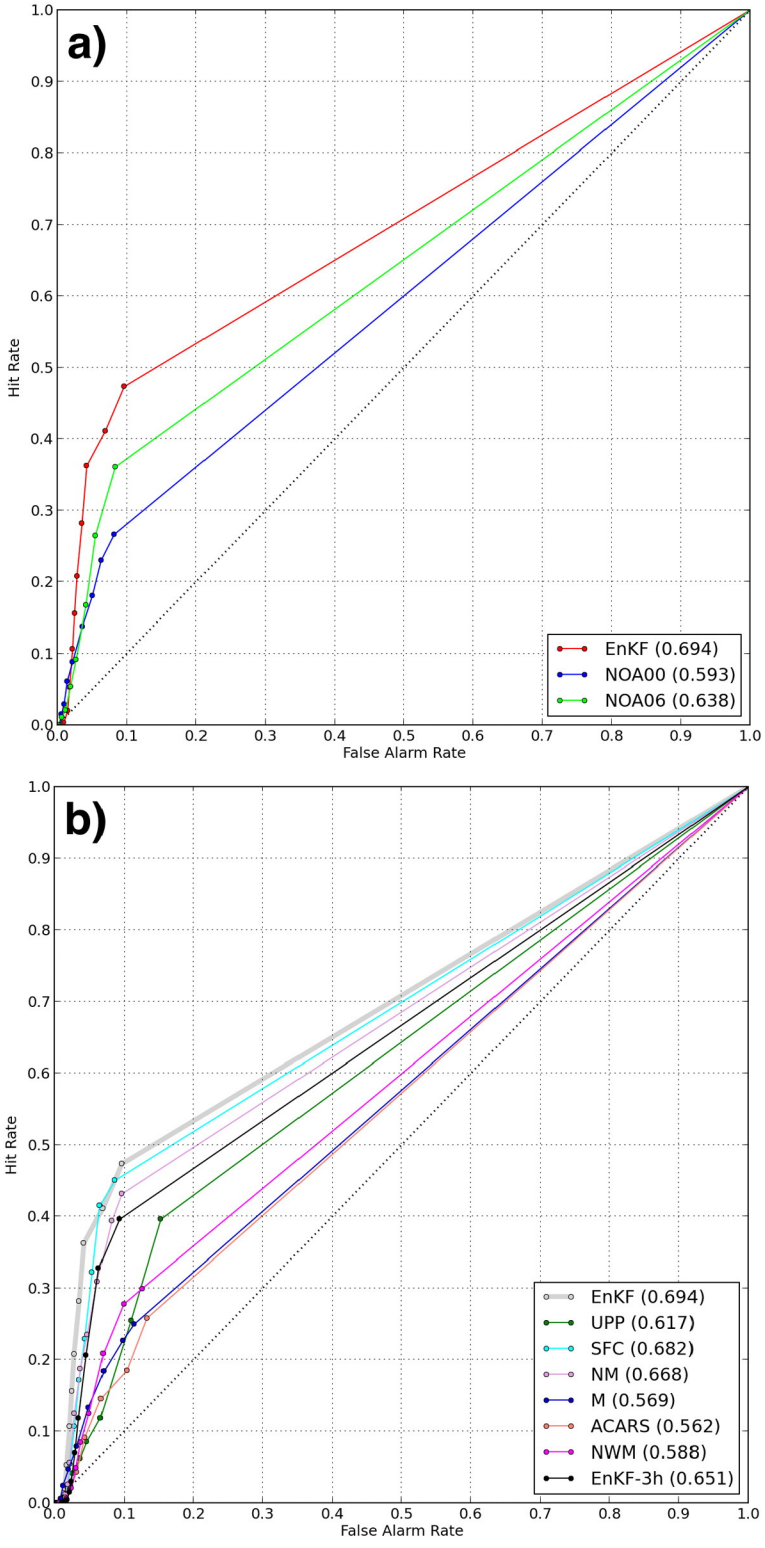

Fig. 11. PoS 06-18 UTC ROC curves and their corresponding AUCs for a) primary experiments; b) sensitivity experiments.

parameters from METARs (NWM, (see Table 3)) in the assimilation. This experiment allows to derive the impact of wind-METAR observations on the PoS field (Fig. 15). Results clearly highlight the positive contribution of wind-METARs over the PoS field, specially along the path followed by the squall line and prominently over the island of Mallorca. Indeed, this notable positive effect is clearly reflected in the AUC (0.69 for EnKF against 0.59 for NWM, (Fig. 11b)).

6. Discussions and conclusions

This paper shows the potential of assimilating conventional observations over the Western Mediterranean Sea using an ensemble Kalman filter technique and test its potential to advect meteorological information from areas with good coverage to areas with lack of observations. In order to explore the benefits of assimilating observations on the

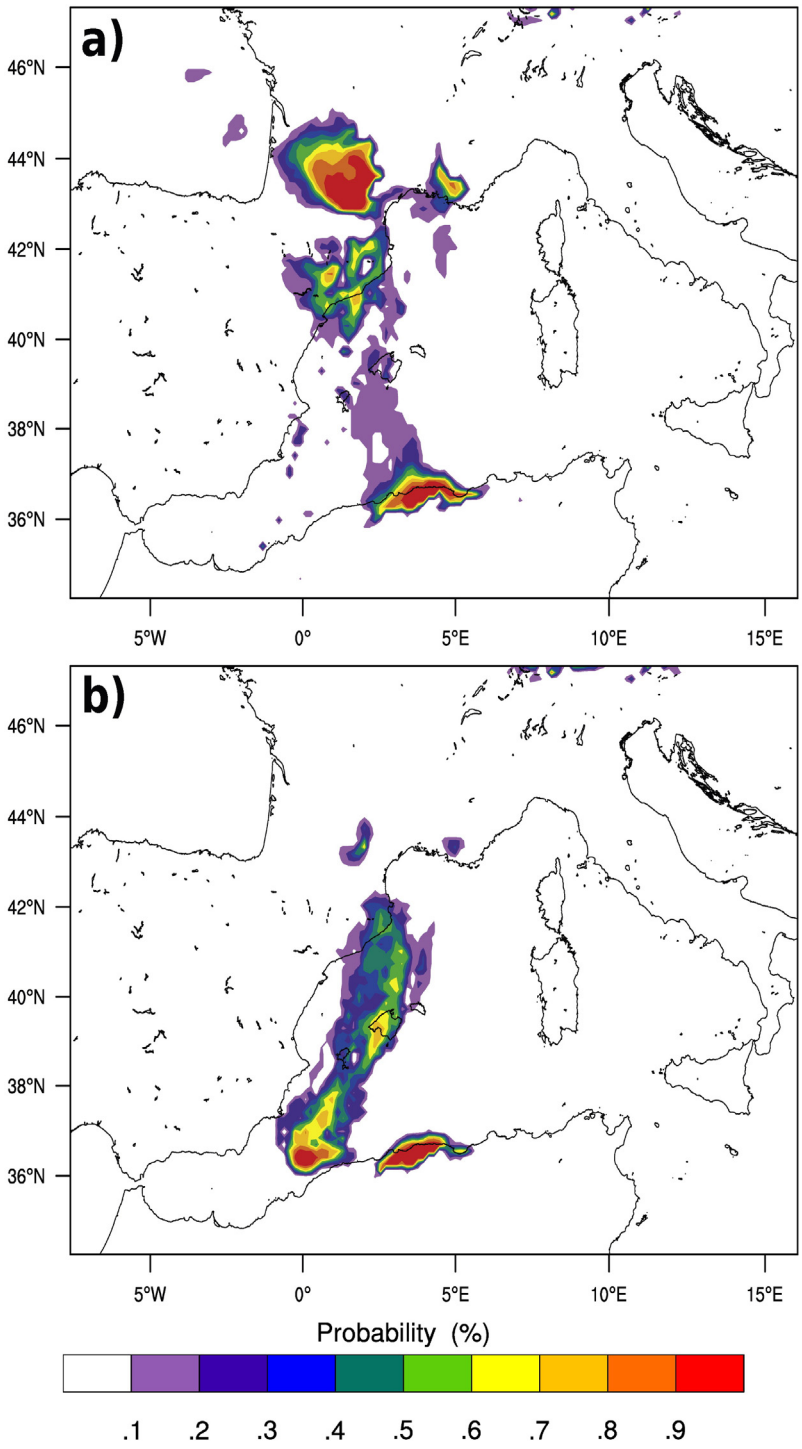

Fig. 12. As in Fig. 6, but for a) UPP and b) SFC experiments.

predictability of Mediterranean severe weather, we study the squall line that affected Mallorca on 4th October 2007 using an EnKF and basic ensemble generation techniques.

Probabilistic forecasts of severe threat show that EnKF experiments better depict the observed path of the squall line and the high probabilities of severe weather over Mallorca, in agreement with observations and AEMET reports. This experiment renders high values of PoS over the Alboran Sea, where the initiation of the convective systems that later on organized as a squall line, was observed. Most ensemble members show intense convective activity over this area and their posterior evolution towards the northeast, sweeping across Mallorca. On the contrary, NOA00 and NOA06 members, do not exhibit such valuable prediction. Only few members depict some convective activity over the Alboran Sea and most often, the simulated thunderstorm path-evolution is shifted westward or evolves in an unrealistic way.

Discrepancies between experiments can be linked to the environments simulated by each ensemble. All three ensembles reproduce analogous thermodynamical environments which favour the actual initiation and sustainment of convection and the later organization into a squall line with high low-level shear and conditional instability values. It is shown that EnKF experiment does not have a relevant impact on the simulated thermodynamical environment. In agreement with Cohuet et al.

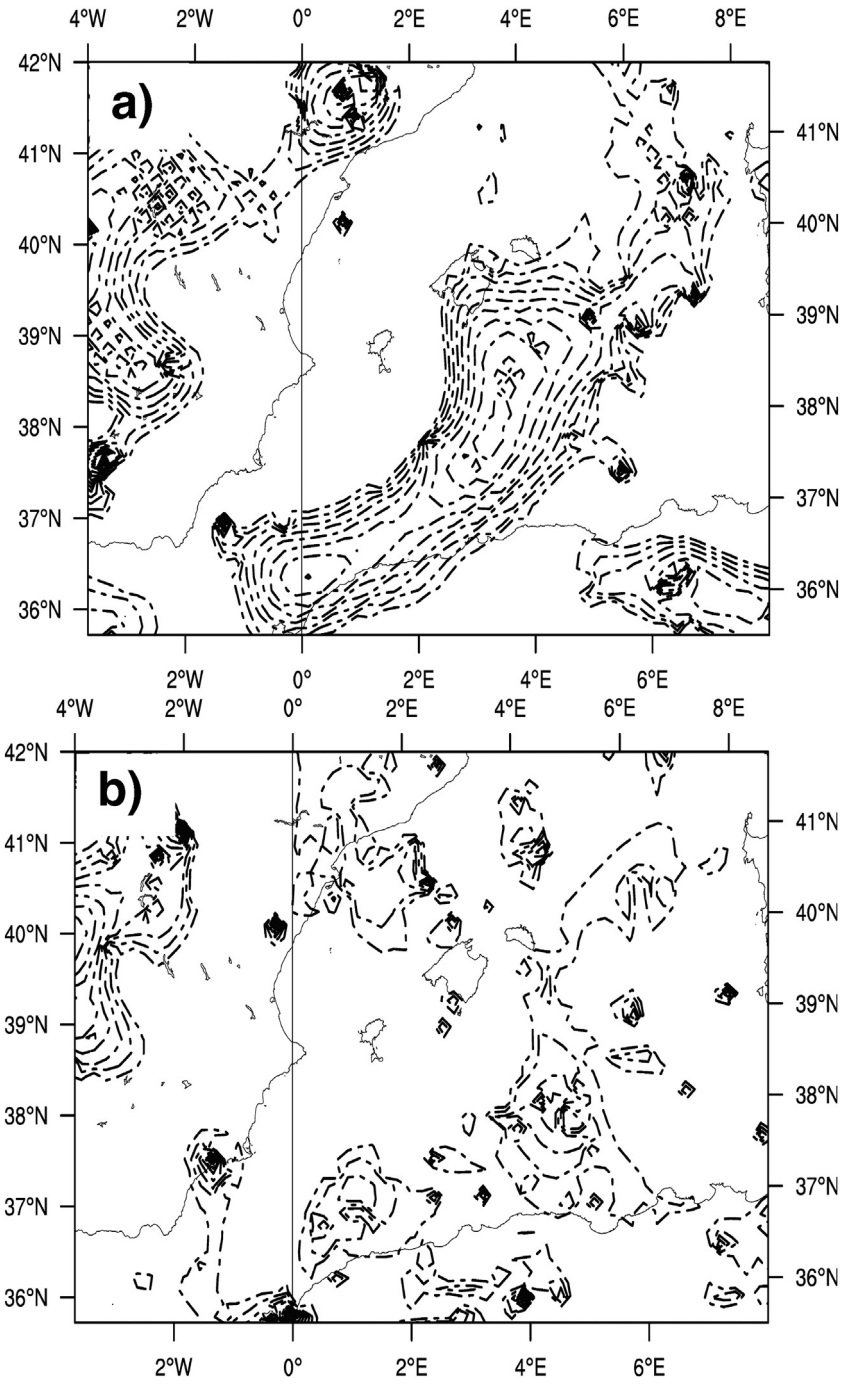

Fig. 13. Difference in probability of convergence between EnKF and a) UPP (e.g. effect of surface observations); b) SFC (e.g. effect of upper air observations).

(2011), we focus the analyses on the low-level divergence field as the key triggering mechanism for the thunderstorm. Only the cycling assimilation EnKF experiment predicts an appreciable zone of convergence over the Alboran Sea, with no discernible signal of it in the NOA00 or NOA06 results. This represents the most explicit evidence of the benefits of assimilating new information sources in the numerical prediction system when dealing with convective activity over maritime data-void regions. Unquestionably, the guidance to stakeholders and civil protection managers would had been much more effective and valuable with the EnKF results than with the NOA00 and NOA06 experiments.

With the aim of associating these forecast improvements to the type of observations (vertical profile and surface) assimilated, additional sensitivity experiments were performed. Assimilating only surface observations suffices to provide the key dynamical aspects that configure the low-level flow and its convergence over the right position. On the other hand, when only vertical profiles are ingested, the ensemble does not provide a dependable description of the severe threat for the episode. To extend these interesting sensitivity experiments and with the purpose of identifying which type of observations contribute the most to this improvement, an extra experiment was performed. Results attribute to the METAR-wind observations the most valuable source of assimilated information to represent the convergence zone and the severe convective environment.

Regarding the individual effect of terrestrial and maritime observations, we applied the factors separation technique to isolate not only the influence of the individual effects but also their synergy. Also, we

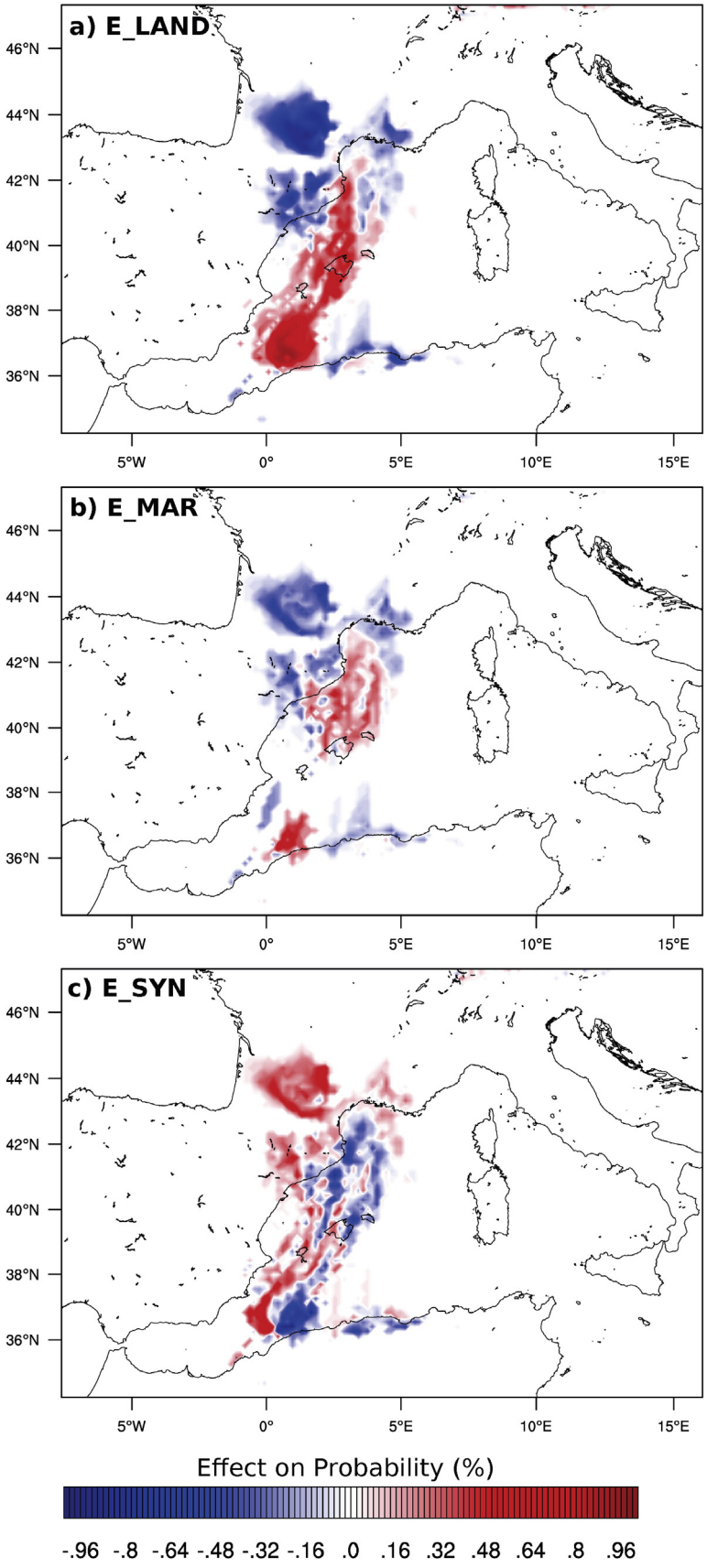

Fig. 14. Effect on the probability of severe in the period 06-18 UTC attributable to (a) land, (b) maritime observations and (c) their synergism.

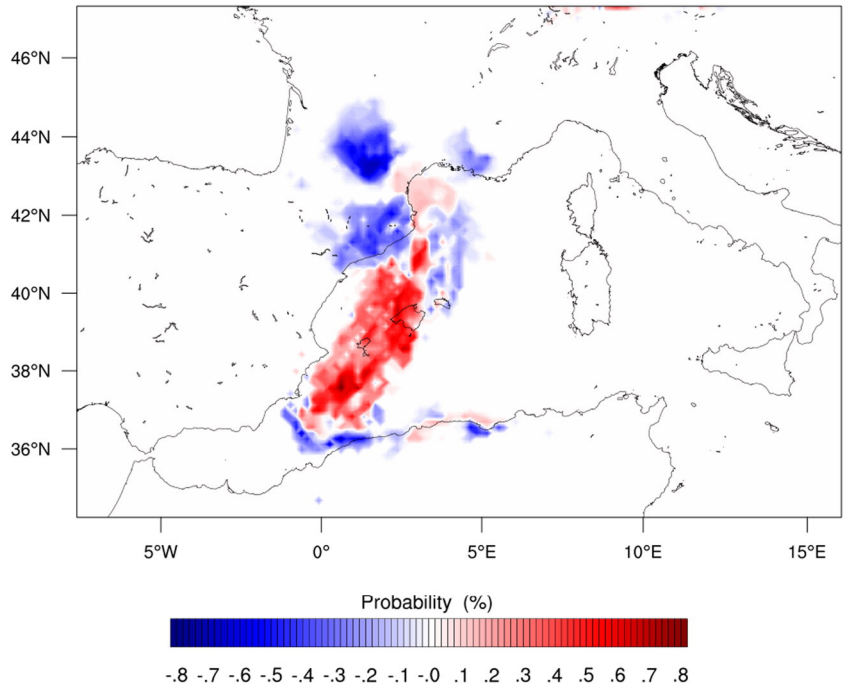

Fig. 15. Effect on the probability of severe in the period 06-18 UTC for wind-METAR observations.

quantify the impact of the assimilation update frequency, concluding that hourly updates of conventional observations still contribute significantly to the probabilistic forecasts of severe weather.

These numerical results confirm the hypothesized conceptual model of observational information from surface stations over land being transported and disseminated towards less densely observed maritime bodies. These results point the way for a significant improvement in the forecast of hazardous weather episodes in coastlands frequently affected by convective systems of maritime origin. This is specially relevant in densely populated regions such as the Mediterranean, highly vulnerable to heavy precipitation and intense winds. The ability of cycling data assimilation methods to transport information from relatively well instrumented areas towards maritime regions set the fundamental motivation for the experiments presented in this paper as not only improves the prediction, as unequivocally shown, but it allegedly can help advance in better distilling and optimizing the use of the massive amount of data collected by satellites over the sea. The combined use of both standard and satellite observations, and the analyses of their impact on the predictability of Mediterranean high-impact weather events remain as the next future challenge to be faced.

Acknowledgements

Lightning strokes distribution and radar images were provided by Agencia Estatal de Meteorología of Spain (AEMET). The authors acknowledge AEMET for supplying these images. Satellite images were obtained from EUMETSAT. The valuable information and technical assistance with the DART software package provided by Nancy Collins is acknowledged. This research is framed within the CGL2011-24458 and CGL2014-52199-R Spanish projects and it has also been partially funded by the Government of the Balearic Islands through the 'Grups Competitius' project 7/2011 of the Conselleria d'Educació, Cultura i Universitats.

References

Anderson, J.L., 2001. An ensemble adjustment Kalman filter for data assimilation. Mon. Weather Rev. 129 (12).

Anderson, J.L., Anderson, S.L., 1999. A Monte Carlo implementation of the nonlinear filtering problem to produce ensemble assimilations and forecasts. Mon. Weather Rev. 127 (12).

Anderson, J., Hoar, T., Raeder, K., Liu, H., Collins, N., Torn, R., Avellano, A., 2009. The data assimilation research testbed: a community facility. Bull. Am. Meteorol. Soc. 90 (9).

Benet, C., 1986. Meteorological data in Sabadell 1897-1979. Ajuntament de Sabadell, Pl. Sant Roc 2.

Bouttier, F., Kelly, G., 2001. Observing-system experiments in the ECMWF 4D-Var data assimilation system. Q. J. R. Meteorol. Soc. 127 (574).

Bowman, A.W., Azzalini, A., 1997. Applied Smoothing Techniques for Data Analysis: The Kernel Approach with S-Plus Illustrations: The Kernel Approach with S-Plus Illustrations. Oxford University Press.

Brousseau, P., Desroziers, G., Bouttier, F., Chapnik, B., 2014. A posteriori diagnostics of the impact of observations on the arome-france convective-scale data assimilation system. Q. J. R. Meteorol. Soc. 140 (680).

Buehner, M., Houtekamer, P., Charette, C., Mitchell, H., He, B., 2009. Intercomparison of variational data assimilation and the Ensemble Kalman Filter for global deterministic NWP. Part I: Description and single-observation experiment. Mon. Weather Rev. 138 (5).

Buizza, R., Houtekamer, P., Pellerin, G., Toth, Z., Zhu, Y., Wei, M., 2005. A comparison of the ECMWF, MSC, and NCEP global ensemble prediction systems. Mon. Weather Rev. 133 (5).

Burgers, G., Jan van Leeuwen, P., Evensen, G., 1998. Analysis scheme in the ensemble Kalman filter. Mon. Weather Rev. 126 (6).

Cacciamani, C., Cesari, D., Grazzini, F., Paccagnella, T., Pantone, M., 2000. Numerical simulation of intense precipitation events south of the Alps: sensitivity to initial conditions and horizontal resolution. Meteorog. Atmos. Phys. 72 (2-4).

Clarke, A., Uehara, T., Porter, J., 1997. Atmospheric nuclei and related aerosol fields over the Atlantic: clean subsiding air and continental pollution during ASTEX. J. Geophys. Res. 102 (D21).

Cohuet, J., Romero, R., Homar, V., Ducrocq, V., Ramis, C., 2011. Initiation of a severe thunderstorm over the Mediterranean Sea. Atmos. Res. 100 (4).

Courtier, P., Andersson, E., Heckley, W., Vasiljevic, D., Hamrud, M., Hollingsworth, A., Rabier, F., Fisher, M., Pailleux, J., 1998. The ECMWF implementation of three-dimensional variational assimilation (3D-Var). I: Formulation. Q. J. R. Meteorol. Soc. 124 (550).

Doswell III, C.A., Brooks, H.E., Maddox, R.A., 1996. Flash flood forecasting: an ingredients-based methodology. Weather Forecast. 11 (4).

Dowell, D.C., Zhang, F., Wicker, L.J., Snyder, C., Crook, N.A., 2004. Wind and temperature retrievals in the 17 May 1981 Arcadia, Oklahoma, supercell: Ensemble Kalman Filter experiments. Mon. Weather Rev. 132 (8).

Ducrocq, V., Nuissier, O., Ricard, D., Lebeaupin, C., Thouvenin, T., 2008. A numerical study of three catastrophic precipitating events over southern France. II: Mesoscale triggering and stationarity factors. Q. J. R. Meteorol. Soc. 134 (630).

Evensen, G., 1994. Sequential data assimilation with a nonlinear quasi-geostrophic model using Monte Carlo methods to forecast error statistics. JGR Oceans 99 (C5).

Fernández, C., Gaertner, M., Gallardo, C., Castro, M., 1995. Simulation of a long-lived meso-β scale convective system over the Mediterranean Coast of Spain. Part I: Numerical predictability. Meteorog. Atmos. Phys. 56 (3-4).

Fujita, T.T., 1981. Tornadoes and downbursts in the context of generalized planetary scales. J. Atmos. Sci. 38 (8).
Fujita, T., Stensrud, D.J., Dowell, D.C., 2007. Surface data assimilation using an ensemble Kalman filter approach with initial condition and model physics uncertainties. Mon. Weather Rev. 135 (5).
Furrer, R., Bengtsson, T., 2007. Estimation of high-dimensional prior and posterior covariance matrices in Kalman filter variants. J. Multivar. Anal. 98 (2).
Gallagher III, F.W., Beasley, W.H., Bohren, C.F., 1996. Green thunderstorms observed. Bull. Am. Meteorol. Soc. 77 (12).
García-Dana, F., Font, R., Rivera, A., 1982. Situación meteorológica durante el episodio de lluvia intensa en el levante español durante Octubre de 1982 ((in Spanish), INM, 68 pp. Available from: Instituto Nacional de Meteorología, Apartado 285).
García-Moya, J.-A., Callado, A., Escribà, P., Santos, C., Santos-Muñoz, D., Simarro, J., 2011. Predictability of short-range forecasting: a multimodel approach. Tellus 63 (3).
Garcies, L., Homar, V., 2009. Ensemble sensitivities of the real atmosphere: application to Mediterranean intense cyclones. Tellus 61 (3).
Gaspari, G., Cohn, S.E., 1999. Construction of correlation functions in two and three dimensions. Q. J. R. Meteorol. Soc. 125 (554).
Gayà, M., Solio, A., 1993. Tornadoes and Downbursts in Menorca (in Catalan. Rev. de Menorca.
Hacker, J.P., Anderson, J.L., Pagowski, M., 2007. Improved vertical covariance estimates for ensemble-filter assimilation of near-surface observations. Mon. Weather Rev. 135 (3).
Hohenegger, C., Schär, C., 2007. Predictability and error growth dynamics in cloud-resolving models. J. Atmos. Sci. 64 (12).
Homar, V., Romero, R., Ramis, C., Alonso, S., 2002. Numerical study of the October 2000 torrential precipitation event over eastern Spain: analysis of the synoptic-scale stationarity. Ann. Geophys. 20 (12).
Homar, V., Romero, R., Stensrud, D., Ramis, C., Alonso, S., 2003. Numerical diagnosis of a small, quasi-tropical cyclone over the western Mediterranean: dynamical vs. boundary factors. Q. J. R. Meteorol. Soc. 129 (590).
Hong, S.-Y., Noh, Y., Dudhia, J., 2006. A new vertical diffusion package with an explicit treatment of entrainment processes. Mon. Weather Rev. 134 (9).
Houtekamer, P., Mitchell, H., 1998a. Data assimilation using an Ensemble Kalman Filter technique. Mon. Weather Rev. 126 (3).
Houtekamer, P., Mitchell, H., 2001. A sequential ensemble Kalman filter for atmospheric data assimilation. Mon. Weather Rev. 129 (1).
Houtekamer, P.L., Mitchell, H.L., 1998b. Data assimilation using an ensemble Kalman filter technique. Mon. Weather Rev. 126 (3).
Houtekamer, P.L., Mitchell, H.L., Pellerin, G., Buehner, M., Charron, M., Spacek, L., Hansen, B., 2005. Atmospheric data assimilation with an ensemble Kalman filter: results with real observations. Mon. Weather Rev. 133 (3).
Janjic, Z.I., 1990. The step-mountain coordinate: physical package. Mon. Weather Rev. 118 (7).
Jansa, A., Genoves, A., Picornell, M.A., Campins, J., Riosalido, R., Carretero, O., 2001. Western Mediterranean cyclones and heavy rain. Part 2: Statistical approach. Meteorol. Appl. 8 (1).
Kain, J.S., Fritsch, J.M., 1990. A one-dimensional entraining/detraining plume model and its application in convective parameterization. J. Atmos. Sci. 47 (23).
Kalman, R.E., 1960. A new approach to linear filtering and prediction problems. J. Fluids Eng. 82 (1).
Kalman, R.E., Bucy, R.S., 1961. New results in linear filtering and prediction theory. J. Fluids Eng. 83 (1).
Kistler, R., Collins, W., Saha, S., White, G., Woollen, J., Kalnay, E., Chelliah, M., Ebisuzaki, W., Kanamitsu, M., Kousky, V., et al., 2001. The NCEP-NCAR 50-year reanalysis: monthly means CD-ROM and documentation. Bull. Am. Meteorol. Soc. 82 (2).
Li, X., Pu, Z., 2008. Sensitivity of numerical simulation of early rapid intensification of Hurricane Emily (2005) to cloud microphysical and planetary boundary layer parameterizations. Mon. Weather Rev. 136 (12).
Lorenc, A., 2003. The potential of the ensemble Kalman filter for NWPa comparison with 4D-Var. Q. J. R. Meteorol. Soc. 129 (595).
Malguzzi, P., Grossi, G., Buzzi, A., Ranzi, R., Buizza, R., 2006. The 1966 century flood in Italy: a meteorological and hydrological revisitation. JGR-Atmos. 111 (D24).
Markowski, P., Richardson, Y., 2011. Mesoscale Meteorology in Midlatitudes. vol. 2. John Wiley & Sons.
Marquis, J., Richardson, Y., Markowski, P., Dowell, D., Wurman, J., Kosiba, K., Robinson, P., Romine, G., 2014. An investigation of the Goshen County, Wyoming, tornadic supercell of 5 June 2009 using EnKF assimilation of Mobile Mesonet and radar observations collected during VORTEX2. Part I: Experiment design and verification of the EnKF analyses. Mon. Weather Rev. 142 (2).
Meng, Z., Zhang, F., 2011. Limited-area ensemble-based data assimilation. Mon. Weather Rev. 139 (7).
Miró-Granada, J., 1969. Una granizada excepcional en Mallorca. Geophys. Res. Lett. 18 (2).
Mitchell, H.L., Houtekamer, P., Pellerin, G., 2002. Ensemble size, balance, and model-error representation in an Ensemble Kalman Filter*. Mon. Weather Rev. 130 (11).
Nakanishi, M., Niino, H., 2004. An improved Mellor–Yamada level-3 model with condensation physics: its design and verification. Bound.-Layer Meteorol. 112 (1).
Navascués, B., Calvo, J., Morales, G., Santos, C., Callado, A., Cansado, A., Cuxart, J., Díez, M., del Río, P., Escribà, P., García-Colombo, O., García-Moya, J., Geijo, C., Gutiérrez, E., Hortal, M., Martínez, I., Orfila, B., Parodi, J., Rodríguez, E., Sánchez-Arriola, J., Santos-Atienza, I., Simarro, J., 2013. Long-term verification of {HIRLAM} and {ECMWF} forecasts over southern Europe: history and perspectives of numerical weather prediction at {AEMET}. Atmos. Res. 125126.
Ogura, Y., Chen, Y.-L., 1977. A life history of an intense mesoscale convective storm in Oklahoma. J. Atmos. Sci. 34 (9).
Palmer, T., Hagedorn, R., 2006. Predictability of weather and climate. Observations, Assimilation and the Improvement of Global Weather Prediction—Some Results From Operational Forecasting and ERA-40. Cambridge University Press, Ch.
Pielke, R.A., Mahrer, Y., 1975. Representation of the heated planetary boundary layer in mesoscale models with coarse vertical resolution. J. Atmos. Sci. 32 (12).
Pleim, J.E., 2007. A combined local and nonlocal closure model for the atmospheric boundary layer. Part I: Model description and testing. J. Appl. Meteorol. Climatol. 46 (9).
Rabier, F., 2005. Overview of global data assimilation developments in numerical weather-prediction centres. Q. J. R. Meteorol. Soc. 131 (613).
Ramis, C., Romero, R., 1995. A first numerical simulation of the development and structure of the sea breeze on the island of Mallorca 13 (9).
Ramis, C., Llasat, M.C., Genovés, A., Jansà, A., 1994. The October-1987 floods in Catalonia: synoptic and mesoscale mechanisms. Meteorol. Appl. 1 (4).
Ramis, C., Romero, R., Homar, V., 2009. The severe thunderstorm of 4 October 2007 in Mallorca: an observational study. Nat. Hazards Earth Syst. Sci. 9 (4).
Riosalido, R., 1990. Satellite Characteristics of Mesoscale Convective Systems Over Spain.
Romero, R., Doswell III, C., Ramis, C., 2000. Mesoscale numerical study of two cases of long-lived quasi-stationary convective systems over eastern Spain. Mon. Weather Rev. 128 (11).
Romero, R., Ramis, C., Alonso, S., 1997. Numerical simulation of an extreme rainfall event in Catalonia: role of orography and evaporation from the sea. Q. J. R. Meteorol. Soc. 123 (539).
Romero, R., Ramis, C., Alonso, S., Doswell III, C.A., Stensrud, D.J., 1998. Mesoscale model simulations of three heavy precipitation events in the western Mediterranean region. Mon. Weather Rev. 126 (7).
Romero, R., Ramis, C., Homar, V., 2014. On the severe convective storm of 29 October 2013 in the Balearic Islands: observational and numerical study. Quart. J. Roy. Meteor, Soc.
Schwartz, C.S., Kain, J.S., Weiss, S.J., Xue, M., Bright, D.R., Kong, F., Thomas, K.W., Levit, J.J., Coniglio, M.C., Wandishin, M.S., 2010. Toward improved convection-allowing ensembles: model physics sensitivities and optimizing probabilistic guidance with small ensemble membership. Weather Forecast. 25 (1).
Shen, F., Min, J., Xu, D., 2016. Assimilation of radar radial velocity data with the WRF hybrid ETKF–3dvar system for the prediction of hurricane Ike (2008). Atmos. Res. 169.
Sippel, J.A., Braun, S.A., Zhang, F., Weng, Y., 2013. Ensemble Kalman filter assimilation of simulated HIWRAP Doppler velocity data in a hurricane. Mon. Weather Rev. 141 (8).
Snyder, C., Zhang, F., 2003. Assimilation of simulated Doppler radar observations with an Ensemble Kalman Filter*. Mon. Weather Rev. 131 (8).
Sobash, R.A., Stensrud, D.J., 2013. The impact of covariance localization for radar data on EnKF analyses of a developing MCS: observing system simulation experiments. Mon. Weather Rev. 141 (11).
Stanski, H.R., Wilson, L.J., Burrows, W.R., 1989. Survey of Common Verification Methods in Meteorology. World Meteorological Organization Geneva.
Stein, U., Alpert, P., 1993. Factor separation in numerical simulations. J. Atmos. Sci. 50 (14).
Stensrud, D.J., Wicker, L.J., Xue, M., II, D.T.D., Yussouf, N., Wheatley, D.M., Thompson, T.E., Snook, N.A., Smith, T.M., Schenkman, A.D., Potvin, C.K., Mansell, E.R., Lei, T., Kuhlman, K.M., Jung, Y., Jones, T.A., Gao, J., Coniglio, M.C., Brooks, H.E., Brewster, K.A., 2013. Progress and challenges with warn-on-forecast. 6th European Conference on Severe Storms 2011. Palma de Mallorca, Spain. Atmos. Res. 123.
Tanamachi, R.L., Wicker, L.J., Dowell, D.C., Bluestein, H.B., Dawson, D.T., Xue, M., 2013. EnKF assimilation of high-resolution, mobile Doppler radar data of the 4 May 2007 Greensburg, Kansas, supercell into a numerical cloud model. Mon. Weather Rev. 141 (2).
Torn, R.D., 2010. Performance of a mesoscale ensemble Kalman filter (EnKF) during the NOAA high-resolution hurricane test. Mon. Weather Rev. 138 (12).
Tudurí, E., Ramis, C., 1997. The environments of significant convective events in the Western Mediterranean. Weather Forecast. 12 (2).
Ulanski, S.L., Garstang, M., 1978. The role of surface divergence and vorticity in the life cycle of convective rainfall. Part II: Descriptive model. J. Atmos. Sci. 35 (6).
Uppala, S.M., Kållberg, P., Simmons, A., Andrae, U., Bechtold, V., Fiorino, M., Gibson, J., Haseler, J., Hernandez, A., Kelly, G., et al., 2005. The ERA-40 re-analysis. Q. J. R. Meteorol. Soc. 131 (612).
Van Leeuwen, P., 2010. Nonlinear data assimilation in geosciences: an extremely efficient particle filter. Q. J. R. Meteorol. Soc. 136 (653).
Vich, M., Romero, R., Homar, V., 2011. Ensemble prediction of mediterranean high-impact events using potential vorticity perturbations. part II: Adjoint-derived sensitivity zones. Atmos. Res. 102 (3).
Wheatley, D.M., Yussouf, N., Stensrud, D.J., 2014. Ensemble Kalman Filter analyses and forecasts of a severe mesoscale convective system using different choices of microphysics schemes. Mon. Weather Rev. 142 (9).
Wu, X., Zhang, S., Liu, Z., Rosati, A., Delworth, T., 2013. A study of impact of the geographic dependence of observing system on parameter estimation with an intermediate coupled model. Clim. Dyn. 40 (7-8).
Yussouf, N., Mansell, E.R., Wicker, L.J., Wheatley, D.M., Stensrud, D.J., 2013 Oct.t. The Ensemble Kalman Filter analyses and forecasts of the 8 May 2003 Oklahoma City tornadic supercell storm using single- and double-moment microphysics schemes. Mon. Weather Rev. 141 (10).
Zhang, F., Snyder, C., Sun, J., 2004. Impacts of initial estimate and observation availability on convective-scale data assimilation with an Ensemble Kalman Filter. Mon. Weather Rev. 132 (5).
Zhang, G., Vivekanandan, J., Brandes, E.A., Meneghini, R., Kozu, T., 2003. The shape-slope relation in observed gamma raindrop size distributions: statistical error or useful information? J. Atmos. Ocean. Technol. 20 (8).